HHS Public Access

Author manuscript

Exp Eye Res. Author manuscript; available in PMC 2020 May 01.

Published in final edited form as:

Exp Eye Res. 2019 May ; 182: 109–124. doi:10.1016/j.exer.2019.03.013.

Amelioration of Visual Deficits and Visual System Pathology after Mild TBI with the Cannabinoid Type-2 Receptor Inverse Agonist SMM-189

Natalie M. Guley[1], **Nobel A. Del Mar**[1], **Tyler Ragsdale**[1], **Chunyan Li**[1], **Aaron M. Perry**[1], **B.M. Moore**[3], **Marcia G. Honig**[1], and **Anton Reiner**[1,2]

[1]Department of Anatomy and Neurobiology, The University of Tennessee Health Science Center Memphis, TN 38163

[2]Department of Ophthalmology, The University of Tennessee Health Science Center Memphis, TN 38163

[3]Dept. of Pharmaceutical Sciences, The University of Tennessee Health Science Center Memphis, TN 38163

Abstract

Mild TBI is often accompanied by visual system dysfunction and injury, which is at least partly caused by microglial neuroinflammatory processes initiated by the injury. Using our focal cranial blast mouse model of closed-skull mild TBI, we evaluated the ability of the cannabinoid type-2 (CB2) receptor inverse agonist SMM-189, which biases microglia from the harmful M1 state to the beneficial M2 state, to mitigate visual system dysfunction and injury after TBI. Male C57BL/6 or Thy1-EYFP reporter mice received a closed-head blast of either 0-psi (sham) or 50- psi to the left side of the cranium. Blast mice received vehicle or 6 mg/kg SMM-189 daily beginning 2 hours after blast. Sham mice received vehicle. In some mice, retina and optic nerve/tract were assessed morphologically at 3–7 days after blast, while other mice were assessed functionally by Optomotry 30 days after blast and morphologically at ≥30 days after blast. Mice sacrificed at 3–7 days were treated daily until sacrificed, while those assessed ≥30 days after blast were treated daily for 2 weeks post blast. Axon damage was evident in the left optic nerve and its continuation as the right optic tract at 3 days post blast in vehicle-treated blast mice in the form of swollen axon bulbs, and was accompanied by a significant increase in the abundance of microglia. Testing at 30 days post blast revealed that the contrast sensitivity function was significantly reduced in both eyes in vehicle-treated blast mice compared to vehicle-treated sham blast mice, and axon counts at ≥30 days after blast revealed a ~10% loss in left optic nerve in vehicle-treated blast mice. Left optic nerve axon loss was highly correlated with the left eye deficit in contrast sensitivity.

Corresponding Author: Dr. Anton Reiner, Department of Anatomy & Neurobiology, University of Tennessee Health Science Center, 855 Monroe Ave., Memphis, TN 38163, office: 901-448-8298, fax: 901-448-7193, areiner@uthsc.edu.

Declarations of interest:
none

Immunolabeling at 30 days post blast showed a significant increase in the abundance of microglia in the retinas of both eyes and in GFAP+ Muller cell processes traversing the inner plexiform layer in the left eye of vehicle-treated blast mice. SMM-189 treatment reduced axon injury and microglial abundance at 3 days, and mitigated axon loss, contrast sensitivity deficits, microglial abundance, and Muller cell GFAP upregulation at ≥30 days after blast injury. Analysis of right optic tract microglia at 3 days post blast for Ml versus M2 markers revealed that SMM-189 biased microglia toward the M2 state, with this action of SMM-189 being linked to reduced axonal injury. Taken together, our results show that focal left side cranial blast resulted in impaired contrast sensitivity and retinal pathology bilaterally and optic nerve loss ipsilaterally. The novel cannabinoid drug SMM-189 significantly mitigated the functional deficit and the associated pathologies. Our findings suggest the value of combatting visual system injury after TBI by using CB2 inverse agonists such as SMM-189, which appear to target microglia and bias them away from the pro-inflammatory M1 state, toward the protective M2 state.

Keywords

TBI; visual deficits; microglia; CB2 receptors; cannabinoid therapy

1. Introduction

Visual deficits after mild traumatic brain injury (TBI) are highly common, particularly among survivors of blast injuries (Cockerham et al., 2009, 2011). Notable among the visual impairments are deficits in visual acuity and contrast sensitivity, reduced visual fields, diminished pupil light reflex, and deficits in dark adaptation (Lew et al., 2004, 2007; Du et al., 2005; Goodrich et al., 2007, 2013; Brahm et al., 2009; Cockerham et al., 2009, 2011,2013; Alvarez et al., 2012). Impairments in fixation, pursuit, saccades, vergence, and accommodation are also observed, leading to reading difficulties and double vision (Du et al., 2005; Ciuffreda et al., 2007; Goodrich et al., 2007, 2013; Stelmack et al., 2009; Brahm et al., 2009; Doble et al., 2010; Green et al., 2010). Optic nerve injury has been recognized by fundus photography and optical coherence tomography in individuals with visual deficits from TBI (Cockerham et al., 2009; Goodrich et al., 2013), as has axonal injury in the optic radiation and cranial oculomotor nerves (Lachapelle et al., 2004; Bruce et al., 2006; Cockerham et al., 2009; Caeyenberghs et al., 2010; Jin et al., 2010; Alvarez et al., 2012). Concussive events produce nervous system compression, stretching, and dynamic shear. Axons are more susceptible to injury than are neuronal cell bodies, due to their viscoelastic nature and large surface to volume ratio, and axons within white matter tracts, such as the optic nerve and tract, have been shown to be especially vulnerable. As a result, head trauma produces optic nerve damage, resulting in retinal ganglion cell loss, retinal thinning, and retinal dysfunction, even without accompanying direct eye trauma (Goodrich et al., 2007; Cockerham et al., 2009).

Interventions that effectively limit the visual impairments that individuals experience following a concussion have not been developed (Das et al., 2018; Diaz-Arrastia et al., 2014). Several molecules released by damaged axons and their myelin sheaths, such as ATP and S100b, bind to damage-associated molecular pattern (DAMP) receptors on microglia,

and thereby activate them to the pro-inflammatory M1 state (Madathil et al., 2018). M1-activated microglia typically release inflammatory cytokines and other toxic substances whose actions worsen the outcome after mild TBI (Cao et al., 2012; Patterson et al., 2012; Loane and Kumar, 2016; Donat et al., 2017). As a result, M1 microglial activation is an attractive target for mitigating damage after TBI. We have previously assessed if modulating activated microglia via their cannabinoid type 2 receptors (CB2) provides an effective therapeutic approach (Reiner et al., 2015; Bu et al., 2016; Liu et al., 2017). CB2 receptors are typically expressed at low levels in the brain, with expression in both microglia and neurons (Stempel et al., 2016). Activated microglia, however, rapidly increase their expression of CB2 receptors many fold above that in neurons (Ashton and Glass, 2007; Romero-Sandoval et al., 2008; Stella, 2010; Schomberg and Olson, 2012; Donat et al., 2014), and so drugs acting on CB2 receptors are promising for selectively targeting microglia without accompanying psychotropic effects (Stella, 2010). CB2 inverse agonists in particular represent a unique class of ligands for beneficially modulating microglia to treat TBI (Lunn et al., 2006, 2008). CB2 inverse agonists bind to inactive conformations of the CB2 receptors, which are normally constitutively active, thereby reducing adenylyl cyclase inhibition and thus increasing cAMP production (Atwood et al., 2012). This in turn leads to the downstream activation of protein kinase A, which phosphorylates the cAMP response element binding protein (CREB). Increased phosphorylation and nuclear translocation of CREB then bias activated microglia from the pro-inflammatory M1 state toward the protective M2 state, which apparently underlies the beneficial effects of CB2 inverse agonists (Lunn et al., 2006, 2008; Lawrence and Natoli, 2011; Presley et al., 2015).

We have previously shown that 2 weeks of daily treatment with the selective CB2 inverse agonist SMM-189, which reduces the M1 features and increases the M2 features of human and murine microglia *in vitro* (Presley et al., 2015; Reiner et al., 2015), greatly attenuates the motor and emotional deficits, neuron loss, and electrophysiological abnormalities that are otherwise evident 2–6 weeks after mild TBI (Reiner et al., 2015; Bu et al., 2016; Liu et al., 2017). We also found that SMM-189 treatment increased levels of nuclear pCREB in microglia in the brain systems under study, thereby biasing the microglia toward an M2 state (Bu et al., 2016). In the present study, we examine in more detail the deficit in contrast sensitivity caused by focal cranial blast, the visual system injury that may drive this deficit, and the basis of the SMM-189 rescue of that deficit. As blast TBI damages axons, which in turn leads to microglial activation, we examined these morphological signs of injury in the optic nerve, optic tract and the retina in the first week after trauma, when secondary pathogenic effects can be modulated, to better understand those events and their long term consequences. We found that SMM-189 treatment reduces the short-term pathologies and the significant loss of optic nerve axons that is otherwise found several months later. Taken together, our findings support the efficacy of SMM-189 and its modulation of microglia in mitigating visual system injury and dysfunction after TBI.

2. Methods

2.1. Animals.

Male C57BL/6 mice or male EYFP-reporter mice on a C57BL/6 background (Jackson Laboratories, Bar Harbor, ME) received either 50-psi or sham blast at about 3 months of age, and then were injected for the next two weeks with either SMM-189 or vehicle intraperitoneally (ip). Functional tests were administered at 30 days after blast, and subsequently the mice were perfused with fixative, and eyes, optic nerves and brains collected for histologic evaluation. Some mice were sacrificed at 3–7 days for histologic analysis. EYFP-reporter mice were used to directly image the morphology of a subset of EYFP+ retinal ganglion cell axons at short time points after blast. These mice were obtained from a cross between a floxed Thy1-EYFP reporter mouse and an emx1-Cre driver mouse, whose offspring express EYFP in all Thy1+ cells of the emx1 lineage, as described in our prior studies (Heldt et al., 2014; Reiner et al., 2015; Guley et al., 2016). The floxed Thy1-EYFP reporter mice (purchased from JAX) and emx1-Cre driver mice (purchased from the Mutant Mouse Regional Resource Consortium) were maintained as colonies at UTHSC. All experiments were in compliance with the ARVO statement on the Use of Animals in Ophthalmic and Vision Research, and with NIH and institutional guidelines.

2.2. Blast TBI Device and Blast Administration.

The blast device consists of a modified, horizontally mounted paintball gun that emits a brief high-pressure air blast. The blast pressure was calibrated to 50–60 pounds per square inch (psi) above atmospheric pressure using a pressure transducer. Mice were anesthetized with Avertin (400 mg/kg body weight) and the left side of the cranium between the ear and the eye exposed to a blast, as described in our prior studies (Heldt et al., 2014; Reiner et al., 2015; Guley et al., 2016). Mice that received sham (0-psi) blast were handled in the identical way as blast mice, but a partition was inserted between the tip of the paintball gun barrel and mouse, to prevent the blast from reaching the mouse. Mice recovered and were ambulating by 15–30 minutes after blast.

2.3. SMM-189 and Vehicle Administration.

SMM-189 was prepared as described previously (Reiner et al., 2015; Bu et al., 2016). Mice were given an ip injection of either vehicle or SMM-189 at a dose of 6 mg/kg of body weight beginning at 2 hours after blast. This was repeated at approximately the same time every day for the next 13 days (14 doses in total), except in the case of mice surviving only 3 or 7 days after blast, which received daily treatment with vehicle or SMM-189 until sacrificed. SMM-189 dose was calculated based on a study on a structurally similar tri-aryl CB2 receptor ligand (Fujinaga et al., 2010), with 6 mg/kg estimated to deliver 4.6 μM of SMM-189 to the brain within hours of the ip injection. Given its known CB2 affinity (Presley et al., 2015), this was deemed adequate to achieve receptor activation in brain (Reiner et al., 2015). SMM-189 possesses favorable biopharmaceutical features, since it has good membrane permeability, metabolic stability, and penetration into the brain (Presley et al., 2015). Mice that received blast and vehicle will henceforth be referred to as blast-vehicle or blast-veh mice, mice that received blast and drug as blast-SMM, and sham mice that received vehicle as sham-vehicle or sham-veh. The short hand is used in figure legends.

2.4. Contrast Sensitivity.

Contrast sensitivity threshold functions were obtained by testing at each of 6 spatial frequencies (0.031, 0.064, 0.092, 0.103, 0.192, and 0.272) at one month post blast, using a Cerebral Mechanics OptoMotry system (CerebralMechanics Inc.: www.cerebralmechanics.com) (Prusky et al., 2004; Douglas et al., 2005), as described previously (Reiner et al., 2015; Guley et al., 2016). Contrast sensitivity was then calculated as the reciprocal of the contrast sensitivity threshold at that given spatial frequency. These mice were also used in immunohistochemical studies of retina. In the case of mice whose optic nerves were used for axon counts (see below), some had been used in a previous study on the effects of TBI and SMM-189 on contrast sensitivity thresholds at 0.042 c/d (Reiner et al., 2015), which was conducted using Optometry one month after blast. An 11 additional animals were used in studies of optic nerve, and contrast sensitivity thresholds were determined here for those mice at 0.042 c/d one month after blast using Optomotry.

2.5. Animal Sacrifice.

Mice were deeply anesthetized with avertin (240 mg/kg), the chest opened, and 0.1mL of heparinized saline (800 U.S.P. units/mL) injected into the heart. Mice were then perfused transcardially with 30 ml of 0.9% NaCl in 0.1 M sodium phosphate buffer at pH 7.4 (PB), followed by 60 ml of 4% paraformaldehyde, 0.1 M lysine-0.1 M sodium periodate in 0.1 M PB at pH 7.4 (PLP). Optic nerves were cut just distal to the optic chiasm, brains removed, and optic nerves and eyes left in place in the skull. A pin was inserted longitudinally into the right side of each brain, to help in later distinguishing left and right sides in the brain sections. Brains were placed in PLP overnight, transferred the following day to a 20% sucrose/10% glycerol solution, and stored at 4°C until sectioning. Eyes left *in situ* after perfusion were cauterized on the temporal side of the cornea to mark orientation, infused with PLP, removed from the socket with attached optic nerve, and placed into PLP for 2 hours of post-fixation at 4°C. The lens was then removed leaving the cautery mark intact, and the eye placed in a 20% sucrose and 0.1 M PB solution. A micro-suture was later placed through the cautery mark to enable identification of temporal and nasal sides during embedding for cryostat sectioning. A subset of optic nerves was separated from their attached eye, post-fixed in 4% paraformaldehyde/0.5% glutaraldehyde in 0.1 M PB, for later embedding in plastic and sectioning, and used for axon counts. The mice whose optic nerves were used for axon counts included 33 animals for which we had previously reported the effects of TBI and SMM-189 on contrast sensitivity thresholds at 0.042 c/d (Reiner et al., 2015), as well as 11 additional animals, with comparable contrast sensitivity measurements, as noted above.

2.6. Tissue Sectioning.

Fixed brains were frozen with dry ice, and then sectioned on a sliding microtome in the transverse plane at 35 μm. Eyes to be used for immunolabeling were embedded in O.C.T. (optimum cutting temperature) compound, typically with optic nerve still attached, and sectioned on a Hacker-Bright cryostat at a thickness of 20 μm through the horizontal meridian. Plastic-embedded optic nerves were sectioned transversely at 1 μm, and then

stained with 1% p-phenylenediamine in 50% methanol (PPD), as described in Bricker-Anthony et al. (2014).

2.7. Optic Nerve Axon Counts.

For optic nerve axon quantification, low and high magnification images were captured using an Olympus BH2 series light microscope with S Plan Apochromat objectives, an achromatic condenser (Olympus Corporation, Tokyo, Japan) and SPOT idea ™ camera (Diagnostic instruments, Inc., Sterling Heights, MI) running on SPOT Advanced software (Version 4.6). A low power image of each optic nerve was captured using a 20x objective to measure its cross sectional area and to divide the nerve into quadrants. A high power image of a subfield within each quadrant was then captured near its mid-point so that the images did not overlap or include the edges of the nerve, using a 100x oil immersion objective. The image of each subfield was overlain with a 4×6 grid of twenty-four 100 microns^2 counting boxes, and 2 boxes per row per grid randomly chosen for count axons. For each counting box, axons falling on the north and east lines of the grid were included, but axons on the south and west lines of the grid were not. The total number of axons counted was divided by the total box area counted to calculate an axon density for each quadrant, axon densities for the 4 quadrants were averaged, and the total number of axons estimated by multiplying the optic nerve cross sectional area by the axon density.

2.8. Immunohistochemistry.

Immunohistochemistry was performed on free-floating sections (brain), or cryostat-sectioned slide-mounted sections (eyes) by single or multiple immunofluorescence as follows: 1) 3 5-minute washes in PB (pH7.4); 2) incubation in primary antibody at room temperature for 24 hours; 3) 3 5-minute washes in PB; 4) incubation in secondary antibody at room temperature for 2 hours; and 5) 3 5-minute washes in PB before mounting (brains), drying, and cover-slipping. Primary antibodies were diluted in a solution of 5% normal horse serum (NHS) and 0.8% Triton X-100/0.01% sodium azide/0.1M PB (PBX). Secondary antibodies were fluorophore-conjugated and also diluted with PBX. Immunofluorescence methods have been described in detail in our prior papers (Reiner et al., 2015; Guley et al., 2016). A Zeiss 710 confocal laser-scanning microscope (CLSM) (Carl Zeiss AG, Oberkochen, Germany) was used to image brain and retinal tissue prepared by immunofluorescence. In some cases, sections were stained with DAPI following immunolabeling and then cover-slipped. Retinal images were obtained on the horizontal meridian from the nasal and temporal side of the eye, or the center of the retina in the case of 3-day post blast Iba-1 analysis. Images were obtained with a 20× 0.8NA objective, using the tile capture feature of the Zen software (Carl Zeiss AG, Oberkochen, Germany) in order to visualize large lengths of about a millimeter of retina in a single image. Laser power and gain were adjusted to optimize image quality, and were standardized across all images for a given marker (or combination of markers). Analysis was performed blinded on histologic images using ImageJ software (National Institutes of Health, USA).

2.9. Antibodies Used.

Table 1 lists the primary antibodies and the dilutions used. A description of each antibody and its specificity follows.

SMI-32.—The SMI-32 antibody is a mouse monoclonal antibody (BioLegend #801701) that detects nonphosphorylated heavy (200 kD) neurofilament protein, which is expressed in subsets of neurons and axons in a wide variety of mammals. To produce SMI-32, mice were immunized with homogenates of saline-perfused rat hypothalamus, and hybridoma cells were subsequently generated and screened (Sternberger et al., 1982). SMI-32 was shown to recognize a nonphosphorylated epitope of the 200 kD neurofilament protein. Its specificity has been characterized via Western blots and by variations in staining following trypsin and/or phosphatase digestion of its target antigen (Sternberger and Sternberger, 1983).

Glial Fibrillary Acidic Protein (GFAP).—The anti-GFAP antibody was a rabbit polyclonal antibody (ImmunoStar #22522) generated using GFAP (MW 50 kD) extracted from bovine spinal cord as the immunogen. The manufacturer reports that the antibody selectively immunolabels astrocytes in neural tissue from humans, rats, mice, guinea pigs, hamsters, kangaroos, sheep, cats, and monkeys. It yields the same pattern of immunostaining that is produced with other astrocytic markers (Ouyang et al. 2007). The pattern of immunostaining we observed in the retina with this antibody matches that shown for several other validated antibodies against GFAP (Humphrey et al 1993; Sun et al 2009; Hippert et al., 2015).

Ionized calcium binding adaptor molecule 1 (Iba-1).—The Iba-1 antibody (Wako Chemicals #019–19741) recognizes a single 17 kD band in Western blots of rat brain microglia, primary microglial cultures and transfected COS cells (manufacturer; Imai et al., 1996). This Iba-1 antibody has been verified as a selective marker of microglia in mice, rats and humans, and does not label neurons or astrocytes (Ito et al., 1998). We found it produced a pattern of immunostaining consistent with that shown in prior studies of retina (Gaucher et al., 2007; Langman, 2007; Bosco et al., 2011; Karlstetter et al., 2010) and brain (Yi et al., 2012; Levy et al., 2015).

CD16/32.—The anti-CD16/32 antibody was a rat monoclonal antibody (Abcam #ab25235) that recognizes a conformational epitope shared by CD16 (Fc gamma II receptor) and CD32 (Fc gamma III receptor). These Fc receptors are expressed by immune cells, and in the nervous system are almost exclusively found on microglia (Bae et al., 2012; Walker and Lue, 2015). Elevated CD16/32 on microglia is regarded as typifying their activation to the M1 state (Cao and He, 2013; Walker and Lue, 2015).

CD206.—The anti-CD206 (mannose receptor) antibody was a goat polyclonal antibody generated against the Leu19-Ala1388 sequence of recombinant mouse CD206 (R&D Systems #AF2535). The manufacturer shows it is specific by Western blot of mouse liver for a 180 kD protein corresponding to CD206. CD206 is expressed by microglia in the nervous system (Ohgidani et al., 2017) and elevated CD206 indicates their activation to the M2 state (Cao and He, 2013; Walker and Lue, 2015). Several published studies have used this anti-CD206 antibody and shown its localization to microglia (Gaudet et al., 2016; Hellstrom-Erkenstam et al., 2016; Pena-Philippides et al., 2016).

2.10. Axon Bulbs in the Optic Nerve and Tract.

Axon bulbs were visualized by either SMI-32 immunolabeling in C57BL/6 mice or EYFP immunofluorescence in Thy1-EYFP reporter mice (Reiner et al., 2015; Guley et al., 2016). Confocal images of sections from mice sacrificed 3, 5, and 7 days after blast were analyzed using ImageJ. For analysis of optic tract, the freehand tool was used to outline the entire right optic tract region, and its area was measured. Axon bulbs whose longest dimension was greater than 6.5 μm were then counted by an individual blinded as to treatment condition. The number of bulbs was divided by the area of the optic tract to calculate an axon bulb density for statistical comparisons.

2.11. Microglia in the Optic Tract.

Confocal images of immunofluorescent labeling for Iba-1, CD16/32, and CD206 in the right optic tract were captured to analyze microglial abundance and M1 versus M2 state. To quantify microglial expression of the M1 marker CD16/32 and the M2 marker CD206, we used a method described by McCloy et al. (2014). In brief, individual microglia were circumscribed in the Iba-1 channel using the free-form drawing tool of ImageJ, and their labeling intensities in the CD16/32 and CD206 channels were measured. Five measurements were taken randomly throughout the optic tract over areas with no microglia to determine the average background intensity in the optic tract for each marker. The background intensities were subtracted from the CD16/32 and CD206 values for each cell, respectively, and the ratio of CD16/32 to CD206 expression was calculated. This ratio was then used to categorize each microglial cell as M1-biased (an M1/M2 ratio equal to or above 1.10), M2-biased (M1/M2 ratio equal to or below 0.90), or non-differential (M1/M2 ratio between 1.09 and 0.91). The percent of cells in the three categories was used for statistical comparisons between treatment groups, using chi-square. A total of 61 microglia were analyzed in this manner for sham-vehicle mice, 107 for blast-vehicle mice and 106 for blast-SMM mice.

2.12. Microglia and Müller Cells in the Retina.

The abundance of Iba-1+ microglia was quantified in retinal sections. Cells were only counted if the cell body was clearly visible and the DAPI channel showed an obvious nucleus. The average number of cells per mm length of retina for each eye was used for statistical comparisons. For Iba-1+ microglia, an ~900 μm length of central retina was analyzed for each case at 3 days post blast, while for 30 days post blast separate ~1200μm lengths of nasal and temporal retina were analyzed for each case. No significant differences were noted between temporal and nasal retina for Iba-1+ microglia at 30 days by paired t-tests, and so the results were combined. As increased expression of GFAP in Müller cell processes within the inner plexiform layer of the retina reflects retinal injury, we counted GFAP+ processes that extended past the retinal ganglion cell (RGC) layer along separate ~1200μm lengths of nasal and temporal retina, at both 7 and 30 days post blast. The total length of the retina analyzed was measured, and used to calculate the number of GFAP+ processes per mm length of retina. No significant differences were noted between temporal and nasal retina for GFAP at either time point by paired t-tests, and so nasal and temporal sides were averaged together, and mean number of processes per μm length was used for statistical comparisons.

2.13. Statistical Analysis.

One-way ANOVA followed by planned comparisons using post-hoc Fisher PLSD (Protected Least Significant Difference) tests was used to analyze behavioral and histological data, unless otherwise stated. For contrast sensitivity and optic tract Iba-1+ microglia during the first week post blast, the functions were compared by two-way ANOVA on the entire contrast sensitivity curve across groups or the entire survival period, respectively. Overall ANOVA was significant for the majority of tests (e.g. optic nerve counts), except in cases in which the 50-psi deficit in vehicle-treated mice was relatively small and/or in which rescue with SMM-189 was substantial. Results are presented as mean ± SEM.

3. Results

3.1. Optomotry Assessment of Visual Function

3.1.1. Contrast Sensitivity Function.—The left eye of the vehicle-treated blast mice showed a deficit in contrast sensitivity across all spatial frequencies tested compared to the sham mice. SMM-189 treatment ameliorated the left eye deficit, with the difference between the drug-treated blast group and the vehicle-treated blast group being significant, but not the difference between the drug-treated blast group and the vehicle-treated sham group (Figure 1A). Similarly, a significant difference was found across spatial frequencies for the right eye between the vehicle-treated blast group and the vehicle-treated sham group, although the deficit was less than for the left eye. SMM-189 treatment also ameliorated the right eye deficit, as contrast sensitivity for the drug-treated 50-psi mice differed from that of the vehicle-treated blast group, but not from the sham group (Figure 1B). Thus, the contrast sensitivity function was reduced after 50-psi blast for both eyes, and that deficit was rescued with SMM-189.

3.2. Axonal Pathology and Microglial Activation in the first week after Blast TBI

3.2.1. Optic Nerve.—When axons are stretched or subjected to shear forces, their microtubules are disrupted and axonal transport is impaired, leading to swelling (i.e. the formation of axon bulbs) proximal to the site of injury (Smith et al., 2013). Axon bulbs can be detected by visualizing cytoskeletal and membrane proteins, such as with SMI-32 immunolabeling of nonphosphorylated 200 kD neurofilament proteins (Tang-Schomer et al., 2012; Del Mar et al, 2015), or EYFP+ labeling in EYFP reporter mice (Del Mar et al, 2015; Guley et al., 2016). Because we had previously observed axon bulbs following TBI in our blast model and shown that microglia exacerbate axonal injury (Reiner et al., 2015; Guley et al., 2016), we carefully examined cryostat sections from left eyes that had several mm of optic nerve still attached. As shown by the example in Figure 2, we observed occasional axon bulbs scattered along the intraorbital part of the optic nerve at 3 days after 50-psi blast. Axon bulbs were more common near the origin of the optic nerve, as we showed previously in Guley et al., 2016. Most strikingly, for each of the 5 left eyes with 4–5 mm of attached optic nerve, numerous, large axon bulbs were concentrated in a ~500 μm length of nerve, corresponding to a level somewhat beyond the extraocular muscles and thus within, or slightly past, the bony optic canal. Immunofluorescent staining for Iba-1 showed that the prominent axon bulbs at this level were frequently associated with microglia possessing

large cell bodies and shortened thick processes, which are typically thought to be reactive (Soltys et al., 2001; Davis et al., 2017).

3.2.2. Optic Tract Axon Bulbs.—We next examined the central continuation of the left optic nerve as the right optic tract at 3, 5, and 7 days after blast (Figure 3). Axon bulbs were common in the right optic tract at 3 days after 50-psi blast in vehicle-treated mice (Figure 3B) and decreased in number and size over the next several days (Figure 3E). Bulbs were significantly more abundant in the blast-vehicle mice than in the sham-vehicle mice across the three to seven-day survival period (Figure 3E). We next evaluated the effect of SMM-189 treatment at 3 days after blast, when the density of bulbs is greatest. Bulb abundance in the right optic tract did not differ significantly between the SMM-189 treated blast and sham animals (Figure 3F), and trended toward being significantly less in the SMM-189-treated blast mice than in vehicle-treated blast mice. These results show that the right optic tract displays prominent axon pathology as a consequence of blast, and that pathology is notably rescued by SMM-189. By contrast, axon bulbs were far less common in the left optic tract (the brain continuation of right optic nerve) of vehicle-treated blast mice (Figure 3D), and were therefore not counted.

3.2.3. Modulation of Microglial State in the Right Optic Tract.—To examine the microglial reaction to axonal injury, we focused on 3 days after blast when axon bulbs were at their most abundant. Immunostaining for Iba-1 revealed that microglia in the right optic tract possessed the enlarged cell bodies and retracted processes that are characteristic of activated microglia, and were often found closely associated with axon bulbs (Figure 4A–B). Consistent with the low abundance of axon bulbs in the left optic tract, we observed few reactive microglia (Figure 4D). For SMM-189 treated mice, reactive microglia were less common in the right optic tract than for vehicle-treated blast mice (Figure 4D), similar to our findings for axon bulbs described in the previous section. To determine if treatment with SMM-189 modulates optic tract microglia from an M1 to an M2 state, as it does for cultured microglial cells (Reiner et al., 2015; Presley et al., 2015), we immunostained for Iba-1, CD16/32 (M1 cell surface marker) and CD206 (M2 cell surface marker). Individual Iba-1+ microglial cells were categorized based on their predominant marker, with cells stained at similar intensities for both markers placed into a no-predominance category (Figure 5A–F). The sham mice had the highest percentage of cells with no predominant surface marker (about 22% of their microglia), in contrast to the vehicle-treated blast and SMM-189 treated blast mice for which only ~5% of the microglia were not predominantly M1 or M2 (Figure 5G). About half of the microglia in control vehicle-treated sham animals were M1-biased and ~28% M2-biased. For the vehicle-treated blast mice, ~90% of the microglia were M1-predominant and only 6.5% were M2-predominant. In SMM-189 treated blast animals, M1-predominant microglia were reduced to just below 70% of the total, and M2-biased microglia were increased to ~25.5%. The vehicle-treated blast and SMM-189 treated blast groups were both different from the sham group in the relative abundance of M1 and M2-biased microglia using chi square goodness-of-fit testing ($p<0.0001$ for both) and were also different from one another ($p<0.0001$). That SMM-189 treatment decreased the proportion of M1-predominant microglia, and increased the proportion of M2-predominant microglia in right optic tract, suggests that it biases microglia from the pro-inflammatory M1 state toward

the anti-inflammatory M2 phenotype after TBI. Although M1 to M2 conversion was limited to ~20% of the microglia at 3 days post blast in SMM-189 treated mice, there was a significant negative correlation between the number of axon bulbs and the relative abundance of M2-biased microglia across the cases, suggesting that the biasing of a portion of the microglial population from M1 to M2 state by SMM-189 was beneficial.

3.3. Long-Term Optic Nerve Pathology

3.3.1. Left Optic Nerve Axon Counts.—To further evaluate the long-term consequences of TBI and SMM-189 treatment on optic nerve, we examined another cohort of mice for which contrast sensitivity had been tested at 0.042 c/d at one month post blast and sacrificed the mice one or more months later, after any degenerating axons would have been removed through phagocytosis, and counted the surviving axons. Left optic nerve axon abundance was significantly less in vehicle-treated blast animals compared to vehicle-treated sham animals, but it was not significantly decreased in SMM-189 treated blast animals (Figure 6A–D). The left eyes in the vehicle-treated blast mice whose optic nerves were analyzed here showed a significant increase in contrast sensitivity thresholds compared to vehicle-treated sham mice (36.7% sensitivity threshold for sham-vehicle versus 79.3% sensitivity threshold for blast-vehicle; p=0.000002). SMM-189 treatment resulted in significant rescue of contrast sensitivity threshold (49.9% sensitivity threshold), since the SMM-189 treated blast mice did not differ significantly from sham mice (p=0.100) but differ significantly from vehicle-treated blast mice (p=0.0005). Regression analysis showed that axon abundance in the left optic nerve across mice in all three groups was significantly correlated with that eye's contrast sensitivity threshold, suggesting that the loss of optic nerve axons contributed to the contrast sensitivity threshold increase after 50-psi blast (Figure 6E).

3.3.2. Right Optic Nerve Axon Counts.—Optic nerve axon abundance for right eyes did not differ significantly among vehicle-treated sham, vehicle-treated blast, and SMM-189 treated blast mice (n=13–15 in each group; Figure 6D). Nonetheless, the right eyes in the blast-vehicle-mice showed a significant increase in contrast sensitivity thresholds compared to vehicle-treated sham mice (31.5% for sham-vehicle versus 78.8% for vehicle-treated blast) (p=0.026). SMM-189 treatment produced significant rescue of contrast sensitivity thresholds (51.4%), since the SMM-189 treated blast mice did not differ significantly from vehicle-treated sham mice (p=0.638) and trended toward being significantly less than in vehicle-treated blast mice (p=0.079), despite the absence of significant changes in right optic nerve axon abundance. Contrast sensitivity thresholds did not correlate with the number of axons across the entire right optic nerve sample (Figure 6F), further indicating that right optic nerve axon loss did not contribute to the right eye contrast sensitivity deficit, as might be expected given that there was no significant axon loss in the right optic nerve for vehicle-treated blast mice.

3.4. Retina

To further evaluate visual system injury that might contribute to visual dysfunction after focal cranial blast TBI, and their amelioration by SMM-189, we examined microglial and astrocyte labeling in left and right retina at several time points after blast.

3.4.1. Iba-1+ Microglia 3 days after Blast.—At 3 days after 50-psi blast, microglia in the left retina were more numerous and more intensely labeled for Iba-1, with processes that more commonly spanned several retinal layers than in the left eyes of sham blast mice (Figure 7A–C). By contrast, microglia in the drug-treated mice were less abundant and appeared to have fewer processes, although some still spanned more than one retinal layer. Microglia counts showed that the number of Iba-1+ microglia in the retina of the left eye was significantly greater in vehicle-treated blast than in the vehicle-treated sham blast mice by one-way ANOVA (Figure 7D). With SMM-189 treatment, microglial abundance was significantly decreased compared to vehicle-treated blast mice, but microglia were still more numerous than after sham blast. The right eyes were statistically equivalent for all groups by one-way ANOVA (Figure 7D).

3.4.2. Iba-1+ Microglia 30 days after Blast.—At 30 days after blast, Iba-1+ microglia were less abundant in the left eyes of vehicle-treated blast mice than at 3 days post blast, although they still commonly possessed radially oriented processes spanning retinal layers (Figure 8A–C). Cell counts showed that Iba-1+ microglial cells in the left retina of vehicle-treated blast mice were about half as numerous as at the 3-day time point, yet they were still significantly more abundant than in vehicle-treated sham animals (Figure 8E). Microglial abundance was significantly decreased in the SMM-189 treated blast mice compared to vehicle-treated blast mice, and it was not significantly different than in vehicle-treated sham mice. The increase in retinal Iba-1+ microglia in the left eye of vehicle-treated blast mice was significantly linked to poorer contrast sensitivity performance for the left eye at higher spatial frequencies (Figure 8F), as the percent contrast needed at 0.64 c/d was significantly correlated with microglial abundance for the left eye.

The right eyes of the vehicle-treated blast mice also showed an increase in microglial abundance, compared to vehicle-treated sham mice (Figure 8D, E), which was unexpected, as they had not exhibited any increase at 3 days. Right retina microglial abundance in the SMM-189 treated blast mice was significantly reduced compared to vehicle-treated blast mice, and statistically indistinguishable from vehicle-treated sham right eye. The increase in retinal Iba-1+ microglia for the right eye in vehicle-treated blast mice was significantly linked to poorer contrast sensitivity performance for the right eye at higher spatial frequencies (Figure 8G), as the percent contrast needed at 0.64 c/d was significantly correlated with microglial abundance for the right eye.

3.4.3. GFAP+ Müller Cells.—Retinal GFAP expression is normally relatively confined to the nerve fiber layer of the retina, where it is localized to astrocytes and Müller cell end feet. Consistent with this, GFAP immunolabeling in the retinas in vehicle-treated sham mice was largely limited to the nerve fiber layer, where it tended to be discontinuous. The left eyes were not significantly different in GFAP immunolabeling for any group at 7 days post blast. However, at 30 days after 50-psi blast (Figure 9A–C), numerous GFAP positive processes had penetrated into the inner plexiform layer and sometimes into the outer retina of the left eye, and regions of conspicuous GFAP upregulation were observed in the nerve fiber and ganglion cell layers that appeared to be perivascular. The pattern of GFAP expression in SMM-189 treated blast mice resembled that in sham animals, with little or no

penetration of Müller cell processes past the nerve fiber layer, and little localized GFAP upregulation in the nerve fiber and ganglion cell layers. Quantification of Müller cell process penetration revealed that significantly more GFAP processes extended sclerad from the retinal ganglion cell layer (GCL) in the left eyes of vehicle-treated blast mice than for either vehicle-treated sham or SMM-189 treated blast animals by one-way ANOVA, while vehicle-treated sham and SMM-189 treated blast mice were not significantly different from one another (Figure 9D). GFAP upregulation was highly correlated with a worsening of contrast sensitivity function for left eyes (Figure 9E), as the mean contrast needed to detect the moving bars across spatial frequencies was significantly correlated with the GFAP score, i.e. the more GFAP+ processes, the higher (worse) the contrast sensitivity thresholds. Moreover, the abundance of microglia and the GFAP score for the left eye were significantly correlated (Figure 9F).

In the case of right eyes, no significant differences in GFAP immunolabeling for any group were seen at 7 days post blast, similar to the left eyes. At 30 days after blast, the right eyes had few GFAP-immunolabeled processes penetrating into the inner plexiform layer and resembled sham mice, but GFAP immunolabeling in the nerve fiber and ganglion cell layers tended to be more continuous. For the right eye of SMM-189 treated blast mice, the pattern of GFAP expression resembled that in vehicle-treated sham animals and quantification of GFAP+ Müller cell process penetration into the inner plexiform showed no significant differences between groups (Figure 9D).

4. Discussion

In our previous studies, we showed that focal cranial blast using our model causes deficits in visual acuity and contrast sensitivity, and this is substantially rectified by treatment with the CB2 inverse agonist SMM-189 (Reiner et al., 2015; Guley et al., 2016). Based on our *in vitro* data (Reiner et al., 2015; Presley et al., 2015), we interpreted this benefit to stem from the modulation by SMM-189 of M1-activated microglia toward the M2 state. Our prior studies suggested that damage to the retina and to retinal ganglion cell axons in the optic tract might form the basis of the visual deficits after TBI and mitigation of such damage might mediate the rescue by SMM-189. In the present study, we examined the optic tract, optic nerve, and the retina for pathological changes in more detail, and found that injury to the retina and to ganglion cell axons both appear to contribute to the visual deficits in our model of TBI. Moreover, we have confirmed that rescue of visual deficits and pathology with SMM-189 involves biasing of activated microglia away from the M1 state toward the M2 state.

4.1. Optic Nerve and Tract Pathology Shortly After TBI.

We have previously reported that left-side focal cranial blast TBI results in axonal injury in the form of swollen axon bulbs and activated microglia in the optic nerve and optic tract that are most obvious a few days after the injury (Guley et al., 2016). In the present study, we found that these signs of injury were prominent at three locations. First, injury was prominent as RGC axons exit the retina, traverse the glial lamina, and become myelinated, as described previously (Guley et al., 2016). Axons here may be vulnerable due to the

unique cytoarchitectural and biomechanical features of this region, as is the case in animal models of glaucoma (Bosco et al., 2016; Burgoyne, 2011; Howell et al., 2007). Second, injury was prominent as RGC axons traverse and/or exit the narrow bony optic nerve canal. That axonal injury and microglial activation are especially prominent in this region suggests that the blast pressure wave, as it passes from left to right, displacing the brain rightwards in the cranium, produces significant stretch, stress, and shear forces at this level of the nerve. Interestingly, axons within the bony canal have been shown to be highly vulnerable to compression in osteopetrotic mice (Kondo et al., 2013) and in weight-drop models of TBI (Evanson et al., 2018). Third, injury was prominent as axons in the left optic nerve continue into the right optic tract. This may be a consequence of the shear forces produced by the blast displacing the brain being strongest along interfaces between tissues with different mechanical properties, white and gray matter in this case (Wright et al., 2013; del Mar et al., 2015) and/or to the more peripheral injury to the left optic nerve. In 50-psi blast mice treated with SMM-189, axon bulbs were substantially decreased in size and abundance at 3 days after blast compared to their blast-vehicle counterparts, demonstrating that even only 3 days of SMM-189 treatment reduces the pathology.

Consistent with the distal parts of axons fragmenting as they undergo Wallerian degeneration (Kerschensteiner et al., 2005; del Mar et al., 2015), axon bulbs became progressively smaller and less abundant at 5–7 days after blast. By >30 days, we counted significantly fewer axons in the left optic nerve for blast-vehicle animals as compared with sham controls, but not for blast mice treated with SMM-189. Thus, the axon bulbs observed in the first week post blast may reflect damage that is severe enough to lead to axon loss, and the reduction in axon bulb abundance with SMM-189 is most probably associated with the rescue of left optic nerve axons that would have otherwise have swelled, fragmented, and degenerated. For axons arising from the right eye, the paucity of axon bulbs in the left optic tract at 3–7 days after 50-psi blast in vehicle-treated mice is consistent with the insignificant loss of right optic nerve axons that we observed a month or more later. Our correlational analysis indicates that the left eye deficit in contrast sensitivity after TBI was likely caused in large part by the loss of left optic nerve axons. The rescue of contrast sensitivity for the left eye with SMM-189 treatment thus appears to have notably stemmed from the rescue of axons that would have otherwise degenerated in left optic nerve. By contrast, the right eye contrast sensitivity deficit could have been caused by either retinal injury or optic nerve dysfunction not manifesting as loss per se, or by injury to central visual areas on the blast (left) side of the brain to which the right eye projects. The rescue of the right eye contrast sensitivity deficit with SMM-189 would then have resulted from the amelioration of this injury(ies) and/or dysfunction.

4.2. Retinal Pathology and the Müller Glial Cell Response.

Müller glial cells play several important roles in the retina, including providing trophic factors and structural support, and clearing debris (Bringmann and Wiedemann, 2011). When activated, Müller glial cells increase the expression of GFAP in their processes, such that GFAP immunostaining extends beyond the NFL and RGC layers of the retina, toward the outer retina (Bringmann and Wiedemann, 2011), with the depth of penetrance being roughly correlated with the severity of retinal injury (Kimble et al., 2006). GFAP elevation

can be detected as early as 24 hours after focal retinal injury, but is not obvious for a week or longer when the injury is diffuse (Humphrey et al., 1993; Kimble et al., 2006; Hippert et al., 2015). In our studies, GFAP upregulation was not observed at 7 days after blast, whereas at 30 days post blast we saw a large increase in the left eye, and more continuous GFAP immunolabeling in the NFL and RGC layers for both eyes. GFAP abnormalities were alleviated by SMM-189 for both eyes, and the increase itself was linked to poorer contrast sensitivity performance, indicating that the GFAP increase indeed reflected retinal injury. The GFAP-enrichment in the NFL/GCL for both eyes in vehicle-treated blast mice is consistent with the interpretation that TBI yielded NFL/GCL injury and, for the left eye at least, the increase may reflect injury to RGC cell bodies and axons. The upregulation of GFAP in Müller cell processes traversing the IPL of the left eye suggests that the damage may have extended more deeply is consistent with the left eye inner retinal thinning we previously reported (Reiner et al., 2015).

4.3. Microglial Inflammatory Response.

Given that M1 activation of microglia is one of the secondary events that appears to worsen the outcome after mild TBI (Cao et al., 2012; Patterson et al., 2012; Loane and Kumar, 2016), microglial activation is an attractive target for reducing the secondary damage that can ensue after the initial trauma. We found that, in fact, microglia are activated in the left retina and optic nerve and in the right optic tract in our TBI model. At 3 days of blast, the left retinas showed nearly a tripling of Iba-1+ microglia compared to sham blast eyes, with more present in the outer retina and many of them in the inner retina now having processes that span the INL. By contrast, retinal microglial soma are normally located predominantly in the inner and outer plexiform layers (Langman, 2007), and possess processes that ramify within the same layer as the cell body (Gaucher et al., 2007; Karlstetter et al., 2010). Under pathological conditions, microglia increase in numbers and begin to migrate from their normal location in the inner retina toward the site of injury using the Müller glia as scaffolding in the case of photoreceptor damage or toward the optic nerve head and nerve fiber layer in the case of optic nerve damage (Schnitzer and Scherer, 1990; Karlstetter et al., 2010; Zeng et al., 2000; Wang et al., 2011). Migration toward the outer retina imparts a more radial orientation to the microglial processes (i.e. vitread to sclerad). Thus, microglia in the retina after blast in our model appear to show an inflammatory response to optic nerve injury, given their increased abundance in the IPL, and to outer retinal injury, given their increased radial orientation. Microglia were fewer in SMM-189 treated mice, indicating a mitigation of their activation, although many still possessed radially oriented processes. In vehicle-treated blast animals, at the same 3-day time point that the left eyes showed a significant microglial response, the right eyes showed no such increase. The morphology of microglia in the right eye also appeared similar to that of sham mice, with few radially oriented processes.

At 30 days after blast, the left retina increase in microglial abundance was still evident, albeit diminished by ~50% from day 3 levels, and microglia with radially oriented processes were still more abundant than in sham blast animals. Additionally, a significant increase in microglial abundance was now evident in the right eye. Thus, left side focal cranial blast yielded secondary pathological processes that had a more rapid onset for the left eye than the

right eye, but eventually occurred in both eyes. Although SMM-189 treatment reduced microglial abundance at 30 days post blast, the remaining microglia in many cases possessed morphological features, such as radially oriented processes, similar to those in vehicle-treated blast mice, indicating an ongoing retinal disease process. The microglial activation that was underway by 3 days occurred in concert with prominent axon injury, and was both a response to the injury and worsened the outcome. Similarly, microglial activation in the retina after blast may reflect a response to the milieu and also adversely affect retinal cell health and function. In this regard, the abatement of pathology and dysfunction in tandem with the reduced microglial abundance in the retina by SMM-189 treatment suggests that microglial responses contribute to retinal pathogenesis following TBI. Further indicative of a possible pathogenic role, the microglia increase at 30 days post blast was linked to GFAP upregulation in the retina and poorer contrast sensitivity.

4.4. The M1/M2 Microglial Modulation by SMM-189.

Our prior *in vi*tro and *in vivo* data suggest that the SMM-189 benefit after blast TBI stems from its modulation of microglia away from the M1 state, toward the M2 state (Reiner et al., 2015; Presley et al., 2015; Bu et al., 2016). To further evaluate this, in the present study we used immunolabeling for cell surface markers that distinguish the M1 state (CD16/CD32) from the M2 state (CD206) (Franco and Fernández-Suárez, 2015). CD16 and CD32 are low affinity Fc receptors, which bind to the Fc portion of antibodies and assist phagocytes in ingesting opsonized cells or bacteria (Swanson and Hoppe, 2004). CD206 is also known as the mannose receptor and assists with phagocytosis, but also has important intracellular functions in cytokine expression (Gazi and Martinez-Pomares, 2009) and clearing lysosomal hydrolases during inflammation (Lee et al., 2002). We found that both sets of markers were widely expressed by microglia in the right optic tract of all three blast-treatment groups, consistent with the idea that microglia exist on a continuum and rarely express only M1 markers, only M2 markers, or neither (Franco and Fernández-Suárez, 2015; Morganti et al., 2016). We therefore classified microglia based on their relative expression of the two markers into those that showed no predominance, those with M1-predominance, and those with M2-predominance. As expected and consistent with studies by others (Madathil et al., 2018), we found that M1-predominant microglia comprised the vast majority of microglia in the vehicle-treated blast animals. M1-predominant microglia were also, however, common in vehicle-treated sham and SMM-189 treated blast mice. In sham mice, nonetheless, microglia with no M1/M2-predominance and with M2-predominance were each about half as common as M1-predominant. By contrast, vehicle-treated blast mice had relatively few no-predominance or M2-predominant microglia (~5% each). Thus, vehicle-treated blast mice had almost a complete conversion of M0 (quiescent) and M2-predominant microglia into M1-predominant microglia. SMM-189 treatment converted about 20% of the M1 microglia present after blast into M2-predominant microglia. Thus, the drug biases many microglia from M1 to M2, and ~20% ‘conversion’ may be enough for a therapeutic effect. Our M1/M2 studies, however, assessed microglia after only 3 days of treatment, when axon bulb formation is at its peak. Since the treatment duration used for functional assessments and long-term morphological assessments was for 2 weeks, it may be that a greater proportion of microglia were converted to the M2 state with more prolonged treatment. Under any circumstance, a higher dose or more frequent dosing than used here might increase the

benefit by converting more M1 microglia to the M2 state. Importantly, the high negative correlation of axon bulb abundance with M2-predominant microglial abundance in right optic tract in SMM-189 treated blast mice at 3 days post blast suggests that the increase in M2 microglia associated with drug treatment may be protective against the axon damage reflected by bulb formation.

The classical view of microglia as having two distinct polarization states has long been understood to be an oversimplification, but its usefulness in providing a simple nomenclature that fits with the role of microglia as either pro- or anti-inflammatory has perpetuated its existence (Hanisch, 2013; Franco and Fernández-Suárez, 2015). Dichotomy into either an M1 or M2 polarization state for activated microglia, however, clearly did not occur in our study. Almost all microglia had a level of CD16/32 expression higher than that of background, indicating at least a low level of M1 marker expression even in M2-predominant microglia. Other recent studies have also found that many microglia co-express surface markers that are classically defined as being M1 and M2-specific (Peferoen et al., 2015; Xu et al., 2016; Morganti et al., 2016). As a result, some researchers have posited that microglia exist on a continuum, with M1 and M2 states representing the ends of this spectrum (Franco and Fernández-Suárez, 2015). We found it somewhat surprising that the sham mice in our study also possessed many microglia that were either M1 or M2 marker predominant. One possible explanation for this is that the stress of handling and daily ip injection of vehicle for two weeks may have led to low-level systemic inflammation, which is known to activate brain microglia (Godbout et al., 2005). Alternatively, it may be that even “resting” microglia express some level of cell surface receptors normally attributed to an activated phenotype (Cherry et al., 2014). In any case, division of microglial states into mutually exclusive M0, M1, and M2 states appears to be a convenient, albeit misleading, oversimplification of microglial state and behavior.

5. Conclusions

The present studies show that contrast sensitivity loss after TBI using our focal cranial blast model is associated with optic nerve axon loss and retinal pathology for the left eye, while the visual deficits for the right eye are likely to arise from retinal and/or brain dysfunction. Activation of microglia to an M1-predominant state appears to be involved in the secondary injury that ensues from TBI. Two weeks of post-TBI SMM-189 treatment significantly improves visual function, attenuates retinal and optic nerve pathology, and biases microglia away from the M1-predominant and toward a more M2-predominant state. Thus, CB2 inverse agonist therapy, in this case with SMM-189, continues to show promise as an approach for alleviating visual system injury and dysfunction after mild TBI.

Acknowledgements

Special thanks to Marion Joni and Josh Rogers for technical assistance and Dr. Patrick Guley for advice during the course of our studies.

Funding Sources

This work was supported by The University of Tennessee Neuroscience Institute (AR, NMG), The Office of the Dean of the College of Medicine at The University of Tennessee Health Science Center (AR), The Office of the

Dean of the College of Graduate Health Sciences at The University of Tennessee Health Science Center (NMG), The Methodist Hospitals Endowed Professorship in Neuroscience (AR), The College of Pharmacy (BMM), and NIH grant EY-005298 (AR). The funding sources played no role in the design or execution of the study, or in the choice of journal for publication.

References

Alvarez TL, Kim EH, Vicci VR, Dhar SK, Biswal BB, Barrett AM. 2012 Concurrent vision dysfunctions in convergence insufficiency with traumatic brain injury. Optom Vis Sci 89:1740–1751. [PubMed: 23190716]

Ashton JC, Glass M. 2007 The cannabinoid CB2 receptor as a target for inflammation-dependent neurodegeneration. Current Neuropharmacol 5:73–80.

Atwood BK, Straiker A, Mackie K. 2012 CB2: therapeutic target-in-waiting. Progress Neuro-Psychopharmacol Biol Psychiat 38:16–20.

Bae EJ, Lee HJ, Rockenstein E, Ho DH, Park EB, Yang NY, Desplats P, Masliah E, Lee SJ. 2012 Antibody-aided clearance of extracellular a-synuclein prevents cell-to-cell aggregate transmission. J Neurosci 32:13454–13469. [PubMed: 23015436]

Bosco A, Steele MR, Vetter ML. 2011 Early microglia activation in a mouse model of chronic glaucoma. J Comp Neurol 519:599–620. [PubMed: 21246546]

Bosco A, Breen KT, Anderson SR, Steele MR, Calkins DJ, Vetter ML. 2016 Glial coverage in the optic nerve expands in proportion to optic axon loss in chronic mouse glaucoma. Exp Eye Res 150:34–43. [PubMed: 26851485]

Brahm KD, Wilgenburg HM, Kirby J, Ingalla S,Chang CY, Goodrich GL. 2009 Visual impairment and dysfunction in combat-injured service members with traumatic brain injury. Optom Vis Sci 86:817–825. [PubMed: 19521270]

Bricker-Anthony C, Hines-Beard J, Rex TS. 2014 Molecular changes and vision loss in a mouse model of closed-globe blast trauma. Invest Ophthalmol Vis Sci 55:4853–4862. [PubMed: 24994864]

Bringmann A, Wiedemann P. 2011 Müller glial cells in retinal disease. Ophthalmologica 227:1–19. [PubMed: 21921569]

Bruce BB, Zhang X, Kedar S, Newman NJ, Biousse V. 2006 Traumatic homonymous hemianopia. J Neurol Neurosurg Psychiatry 77:986–988. [PubMed: 16574725]

Bu W, Ren H, Deng Y, Del Mar N, Guley N, Moore B, Honig MG, Reiner A 2016 Mild traumatic brain injury produces neuron loss that can be rescued by modulating microglial activation using a CB2 receptor inverse agonist. Front Neurosci 10: 449. [PubMed: 27766068]

Burgoyne CF. 2011 A biomechanical paradigm for axonal insult within the optic nerve head in aging and glaucoma. Exp Eye Res 93:120–132. [PubMed: 20849846]

Caeyenberghs K, Leemans A, Geurts M, Taymans T, Vander Linden C, Smits-Engelsman BC, Sunaert S, Swinnen SP. 2010 Brain-behavior relationships in young traumatic brain injury patients: fractional anisotropy measures are highly correlated with dynamic visuomotor tracking performance. Neuropsychologia 48:1472–1482. [PubMed: 20117121]

Cao L, He C. 2013 Polarization of macrophages and microglia in inflammatory demyelination. Neurosci Bull 29:189–198. [PubMed: 23558588]

Cao T, Thomas TC, Ziebell JM, Pauly JR, Lifshitz J. 2012 Morphological and genetic activation of microglia after diffuse traumatic brain injury in the rat. Neuroscience 225:65–75. [PubMed: 22960311]

Cherry JD, Olschowka JA, O'Banion MK. 2014 Neuroinflammation and M2 microglia: the good, the bad, and the inflamed. J Neuroinflamm 11:98.

Ciuffreda KJ, Kapoor N, Rutner D, Suchoff IB, Han ME, Craig S. 2007 Occurrence of oculomotor dysfunctions in acquired brain injury: a retrospective analysis. Optometry 78:155–161. [PubMed: 17400136]

Cockerham GC, Goodrich GL, Weichel ED, Orcutt JC, Rizzo JF, Bower KS, Schuchard RA. 2009 Eye and visual function in traumatic brain injury. J Rehabil Res Dev 46:811–818. [PubMed: 20104404]

Cockerham GC, Rice TA, Hewes EH, Cockerham KP, Lemke S, Wang G, Lin RC, Glynn-Milley C, Zumhagen L. 2011 Closed-eye ocular injuries in the Iraq and Afghanistan Wars. N Engl J Med. 364:2172–2173. [PubMed: 21631351]

Cockerham GC, Lemke S, Glynn-Milley C, Zumhagen L, Cockerham KP. 2013 Visual performance and the ocular surface in traumatic brain injury. Ocul Surf 11:25–34. [PubMed: 23321357]

Das M, Tang X, Mohapatra SS, Mohapatra S. 2018 Vision impairment after traumatic brain injury: present knowledge and future directions. Rev Neurosci pii: /j/revneuro.ahead-of-print/revneuro-2018-0015/revneuro-2018-0015.xml. [Epub ahead of print]

Davis BM, Salinas-Navarro M, Cordeiro MF, Moons L, De Groef L. 2017 Characterizing microglia activation: a spatial statistics approach to maximize information extraction. Sci Rep 7:1576. [PubMed: 28484229]

Del Mar N, von Buttlar X, Yu AS, Guley NH, Reiner A, Honig MG. 2015 A novel closed-body model of spinal cord injury caused high-pressure air blasts produces extensive axonal injury and motor impairments. Exp Neurol. 271: 53–71. [PubMed: 25957630]

Diaz-Arrastia R, Kochanek PM, Bergold P, Kenney K, Marx CE, Grimes CJ, Loh LT, Adam LT, Oskvig D, Curley KC, Salzer W. 2014 Pharmacotherapy of traumatic brain injury: state of the science and the road forward: report of the Department of Defense Neurotrauma Pharmacology Workgroup. J Neurotrauma 31:135–158. [PubMed: 23968241]

Doble JE, Feinberg DL, Rosner MS, Rosner AJ. 2010 Identification of binocular vision dysfunction (vertical heterophoria) in traumatic brain injury patients and effects of individualized prismatic spectacle lenses in the treatment of postconcussive symptoms: a retrospective analysis. Physical Med & Rehab 2:244–253.

Donat CK, Fischer F, Walter B, Deuther-Conrad W, Brodhun M, Bauer R, Brust P. 2014 Early increase of cannabinoid receptor density after experimental traumatic brain injury in the newborn piglet. Acta Neurobiol Exp 74:197–210.

Donat CK, Scott G, Gentleman SM, Sastre M. 2017 Microglial Activation in Traumatic Brain Injury. Front Aging Neurosci 9:208. [PubMed: 28701948]

Douglas RM, Alam NM, Silver BD, McGill TJ, Tschetter WW, Prusky GT. 2005 Independent visual threshold measurements in the two eyes of freely moving rats and mice using a virtual-reality optokinetic system. Vis Neurosci 22:677–684. [PubMed: 16332278]

Du T, Ciuffreda KJ, Kapoor N. 2005 Elevated dark adaptation thresholds in traumatic brain injury. Brain Inj 19:1125–1138. [PubMed: 16286326]

Evanson NK, Guilhaume-Correa F, Herman JP, Goodman MD. 2018 Optic tract injury after closed head traumatic brain injury in mice: A model of indirect traumatic optic neuropathy. PLoS One 13(5): e0197346. [PubMed: 29746557]

Franco R, Fernández-Suárez D. 2015 Alternatively activated microglia and macrophages in the central nervous system. Prog Neurobiol 131:65–86. [PubMed: 26067058]

Fujinaga M, Kumata K, Yanamoto K, Kawamura K, Yamasaki T, Yui J, Hatori A, Ogawa M, Yoshida Y, Nengaki N, Maeda J, Zhang MR. 2010 Radiosynthesis of novel carbon-11-labeled triaryl ligands for cannabinoid-type 2 receptor. Bioorg Med Chem Lett 20:1565–1568. [PubMed: 20137936]

Gaucher D, Chiappore JA, Pâques M, Simonutti M, Boitard C, Sahel JA, Massin P, Picaud S. 2007 Microglial changes occur without neural cell death in diabetic retinopathy. Vision Res 47:612–623. [PubMed: 17267004]

Gaudet AD, Mandrekar-Colucci S, Hall JC, Sweet DR, Schmitt PJ, Xu X, Guan Z, Mo X, Guerau-de-Arellano M, Popovich PG. 2016 miR-155 Deletion in mice overcomes neuron-intrinsic and neuron-extrinsic barriers to spinal cord repair. J Neurosci 36:8516–8532. [PubMed: 27511021]

Gazi U, Martinez-Pomares L. 2009 Influence of the mannose receptor in host immune responses. Immunobiology 214:554–561. [PubMed: 19162368]

Godbout JP, Chen J, Abraham J, Richwine AF, Berg BM, Kelley KW, Johnson RW. 2005 Exaggerated neuroinflammation and sickness behavior in aged mice following activation of the peripheral innate immune system. FASEB J. 19, 1329–1331. [PubMed: 15919760]

Goodrich GL, Kirby J, Cockerham G, Ingalla SP, Lew HL. 2007 Visual function in patients of a polytrauma rehabilitation center: a descriptive study. J Rehabil Res Dev 44:929–936. [PubMed: 18075950]

Goodrich GL, Flyg HM, Kirby JE, Chang CY, Martinsen GL. 2013 Mechanisms of TBI and visual consequences in military and veteran populations. Optom Vis Sci 90:105–112. [PubMed: 23314131]

Green W, Ciuffreda KJ, Thiagarajan P, Szymanowicz D, Ludlam DP, Kapoor N. 2010 Accommodation in mild traumatic brain injury. J Rehabil Res Dev 47:183–199. [PubMed: 20665345]

Guley NH, Rogers J, Del Mar N, Deng Y, Islam RM, D'Surney L, Ferrell J, Deng B, Hines-Beard J, Bu W, Ren H, Elberger AJ, Marchetta J, Rex TS, Honig MG, Reiner A. 2016 A novel closed-head model of mild traumatic brain injury using focal primary overpressure blast to the cranium in mice. J Neurotrauma 33: 403–422. [PubMed: 26414413]

Hanisch UK. 2013 Functional diversity of microglia - how heterogeneous are they to begin with? Front Cell Neurosci 7:65. [PubMed: 23717262]

Heldt SA, Elberger AJ, Deng Y, Guley NH, Del Mar N, Rogers J, Choi GW, Ferrell J, Rex TS, Honig MG, Reiner A. 2014 A novel closed-head model of mild traumatic brain injury caused by primary overpressure blast to the cranium produces sustained emotional deficits in mice. Front Neurol 5:2. [PubMed: 24478749]

Hellstrom-Erkenstam N, Smith PLP, Fleiss B, Nair S, Svedin P, Wang W, Boström M, Gressens P, Hagberg H, Brown KL, Sävman K, Mallard C. 2016 Temporal characterization of microglia/macrophage phenotypes in a mouse model of neonatal hypoxic-ischemic brain injury. Frontiers Cell Neurosci 10:286.

Hippert C, Graca AB, Barber AC, West EL, Smith AJ, Ali RR, Pearson RA. 2015 Müller glia activation in response to inherited retinal degeneration is highly varied and disease-specific. PLoS ONE 10(3): e0120415. [PubMed: 25793273]

Howell GR, Libby RT, Jakobs TC, Smith RS, Phalan FC, Barter JW, Barbay JM, Marchant JK, Mahesh N, Porciatti V, Whitmore AV, Masland RH, John SW. 2007 Axons of retinal ganglion cells are insulted in the optic nerve early in DBA/2J glaucoma. J Cell Biol. 179:1523–1537. [PubMed: 18158332]

Humphrey MF, Constable IJ, Chu Y, Wiffen S. 1993 A quantitative study of the lateral spread of Müller cell responses to retinal lesions in the rabbit. J Comp Neurol 334:545–558. [PubMed: 8408765]

Imai Y, Ibata I, Ito D, Ohsawa K, Kohsaka S. 1996 A novel gene iba1 in the major histocompatibility complex class III region encoding an EF hand protein expressed in a monocytic lineage. Biochem Biophys Res Commun 224:855–862. [PubMed: 8713135]

Ito D, Imai Y, Ohsawa K, Nakajima K, Fukuuchi Y, Kohsaka S. 1998 Microglia-specific localisation of a novel calcium binding protein, Iba1. Brain Res Mol Brain Res 57:1–9. [PubMed: 9630473]

Jin H, Wang S, Hou L, Pan C, Li B, Wang H, Yu M, Lu Y. 2010 Clinical treatment of traumatic brain injury complicated by cranial nerve injury. Injury Int J Care Injured 41:918–923.

Karlstetter M, Ebert S, Langmann T. 2010 Microglia in the healthy and degenerating retina: Insights from novel mouse models. Immunobiology 215:685–691. [PubMed: 20573418]

Kerschensteiner M, Schwab ME, Lichtman JW, Misgeld T. 2005 In vivo imaging of axonal degeneration and regeneration in the injured spinal cord. Nature Medicine 11:572–577.

Kimble TD, Fitzgerald ME, Reiner A. 2006 Sustained upregulation of glial fibrillary acidic protein in Muller cells in pigeon retina following disruption of the parasympathetic control of choroidal blood flow. Exp Eye Res 83:1017–1030. [PubMed: 16839546]

Kondo Y, Ramaker JM, Radcliff AB, Baldassari S, Mayer JA, Ver Hoeve JN, Zhang CL, Chiu SY, Colello RJ, Duncan ID. 2013 Spontaneous optic nerve compression in the osteopetrotic (op/op) mouse: a novel model of myelination failure. J Neurosci. 33(8):3514–25. [PubMed: 23426679]

Lachapelle J, Ouimet C, Bach M, Ptito A, McKerral M. 2004 Texture segregation in traumatic brain injury--a VEP study. Vision Res 44:2835–2842. [PubMed: 15342227]

Langmann T 2007 Microglial activation in retinal degeneration. J Leukoc Biol 81:1345–1351. [PubMed: 17405851]

Lawrence T, Natoli G. 2011 Transcriptional regulation of macrophage polarization: enabling diversity with identity. Nat Rev Immunol 11:750–761. [PubMed: 22025054]

Lee SJ, Evers S, Roeder D, Parlow AF, Risteli J, Risteli L, Lee YC, Feizi T, Langen H, Nussenzweig MC. 2002 Mannose receptor-mediated regulation of serum glycoprotein homeostasis. Science 295:1898–1901. [PubMed: 11884756]

Levy C, Brooks JM, Chen J, Su J, Fox MA. 2015 Cell-specific and developmental expression of lectican-cleaving proteases in mouse hippocampus and neocortex. J Comp Neurol 523:629–648. [PubMed: 25349050]

Lew HL, Lee EH, Pan SS, Date ES. 2004 Electrophysiologic abnormalities of auditory and visual information processing in patients with traumatic brain injury. Am J Phys Med Rehabil 83:428–433. [PubMed: 15166686]

Lew HL, Poole JH, Vanderploeg RD, Goodrich GL, Dekelboum S, Guillory SB, Sigford B, Cifu DX. 2007 Program development and defining characteristics of returning military in a VA polytrauma network site. J Rehabil Res Dev 44:1027–1034. [PubMed: 18075959]

Liu Y, McAfee SS, Guley NM, Del Mar N, Bu W, Heldt SA, Honig MG, Moore BM 2nd, Reiner A, DH Heck. 2017 Abnormalities in dynamic brain activity caused by mild traumatic brain injury are partially rescued by the cannabinoid type-2 receptor inverse agonist SMM-189. eNeuro. 18: 4(4).

Loane DJ, Kumar A. 2016 Microglia in the TBI brain: The good, the bad, and the dysregulated. Exp Neuro. 275:316–327.

Lunn C, Fine J, Rojas-Triana A, Jackson J, Fan XD, Kung T, Gonsiorek W, Schwarz M, Lavey B, Kozlowski J, Narula S, Lundell D, Hipkin R, Bober L. 2006 A novel cannabinoid peripheral cannabinoid receptor-selective inverse agonist blocks leukocyte recruitment in vivo. J Pharmacol Exp Ther 316:780–788. [PubMed: 16258021]

Lunn C, Reich E-P, Fine J, Lavey B, Kozlowski J, Hipkin R, Lundell D, Bober L. 2008 Biology and therapeutic potential of cannabinoid CB2 receptor inverse agonists. Br J Pharmacol 153:226–239. [PubMed: 17906679]

Madathil SK, Wilfred BS, Urankar SE, Yang W, Leung LY, Gilsdorf JS, Shear DA. 2018 Early microglial activation following closed-head concussive injury is dominated by pro-inflammatory M-1 type. Front Neurol 9:964. [PubMed: 30498469]

McCloy RA, Rogers S, Caldon CE, Lorca T, Castro A, Burgess A. 2014 Partial inhibition of Cdk1 in G 2 phase overrides the SAC and decouples mitotic events. Cell Cycle 13:1400–1412. [PubMed: 24626186]

Morganti JM, Riparip L-K, Rosi S. 2016 Call off the dog(ma): M1/M2 polarization is concurrent following traumatic brain injury. PLoS ONE 11(1): e0148001. [PubMed: 26808663]

Ohgidani M, Kato TA, Haraguchi Y, Matsushima T, Mizoguchi Y, Murakawa-Hirachi T, Sagata N, Monji A, Kanba S. 2017 Microglial CD206 gene has potential as a state marker of bipolar disorder. Front Immunol 7:676. [PubMed: 28119691]

Ouyang YB, Voloboueva LA, Xu LJ, Giffard RG. 2007 Selective dysfunction of hippocampal CA1 astrocytes contributes to delayed neuronal damage after transient forebrain ischemia. J Neurosci 27:4253–4260. [PubMed: 17442809]

Patterson ZR, Holahan MR. 2012 Understanding the neuroinflammatory response following concussion to develop treatment strategies. Front Cell Neurosci 6:58. [PubMed: 23248582]

Peferoen LA, Vogel DY, Ummenthum K, Breur M, Heijnen PD, Gerritsen WH, Peferoen-Baert RM, van der Valk P, Dijkstra CD, Amor S. 2015 Activation status of human microglia is dependent on lesion formation stage and remyelination in multiple sclerosis. J Neuropathol Exp Neurol 74:48–63. [PubMed: 25470347]

Pena-Philippides JC, Caballero-Garrido E, Lordkipanidze T, Roitbak T. 2016 In vivo inhibition of miR-155 significantly alters post-stroke inflammatory response. J Neuroinflamm 13:28.

Presley C, Abidi A, Suryawanshi S, Mustafa S, Meibohm B, Moore BM. 2015 Pre-clinical evaluation of SMM-189, a cannabinoid receptor-2 specific inverse agonist. Pharmacol Res & Perspect 3: e00159.

Prusky GT, Alam NM, Beekman S, Douglas RM. 2004 Rapid quantification of adult and developing mouse spatial vision using a virtual optomotor system. Invest Ophthalmol Vis Sci. 45:4611–4616. [PubMed: 15557474]

Reiner A, Heldt SA, Presley CS, Guley NH, Elberger AJ, Deng Y, D'Surney L, Rogers JT, Ferrell J, Bu W, Del Mar N, Honig MG, Gurley SN, Moore BM. 2015 Motor, visual and emotional deficits in mice after closed-head mild traumatic brain injury are alleviated by the novel CB2 inverse agonist SMM-189. Int. J. Mol. Sci 16:758–787.

Romero-Sandoval A, Nutile-McMenemy N, DeLeo JA. 2008 Spinal microglial and perivascular cell cannabinoid receptor type 2 activation reduces behavioral hypersensitivity without tolerance after peripheral nerve injury. Anesthesiology 108:722–734. [PubMed: 18362605]

Schnitzer J, Scherer J. 1990 Microglial cell responses in the rabbit retina following transection of the optic nerve. J Comp Neurol 302:779–791. [PubMed: 1964466]

Schomberg D, Olson J. 2012 Immune responses of microglia in the spinal cord:Contribution to pain states. Exp Neurol 234:262–270. [PubMed: 22226600]

Smith DH, Hicks R, Povlishock JT. 2013 Therapy development for diffuse axonal injury. J Neurotrauma. 30(5): 307–323. [PubMed: 23252624]

Soltys Z, Marek Z, Pawlinski R, Setkowicz Z, Janeczko K. 2001 Morphology of reactive microglia in the injured cerebral cortex. Fractal analysis and complementary quantitative methods. J Neurosci Res 63:90–97. [PubMed: 11169618]

Stella N 2010 Cannabinoid and cannabinoid-like receptors in microglia, astrocytes and astrocytomas. Glia 58:1017–1030. [PubMed: 20468046]

Stelmack JA, Frith T, Van Koevering D, Rinne S, Stelmack TR. 2009 Visual function in patients followed at a Veterans Affairs polytrauma network site: an electronic medical record review. Optometry 80:419–424. [PubMed: 19635432]

Stempel AV, Stumpf A, Zhang HY, Özdoğan T, Pannasch U, Theis AK, Otte DM, Wojtalla A, Rácz I, Ponomarenko A, Xi ZX, Zimmer A, Schmitz D. 2016 Cannabinoid type 2 receptors mediate a cell type-specific plasticity in the hippocampus. Neuron 90:795–809. [PubMed: 27133464]

Sternberger LA, Harwell LW, Sternberger NH. 1982 Neurotypy: regional individuality in rat brain detected by immunocytochemistry with monoclonal antibodies. Proc Natl Acad Sci USA 79:1326–1330. [PubMed: 7041117]

Sternberger LA, Sternberger NH. 1983 Monoclonal antibodies distinguish phosphorylated and nonphosphorylated forms of neurofilaments in situ. Proc Natl Acad Sci USA 80:6126–6130. [PubMed: 6577472]

Sun D, Lye-Barthel M, Masland RH, Jakobs TC. 2009 The morphology and spatial arrangement of astrocytes in the optic nerve head of the mouse. J Comp Neurol 516:1–19. [PubMed: 19562764]

Swanson JA, Hoppe AD. 2004 The coordination of signaling during Fc receptor-mediated phagocytosis. J Leukoc Biol 76:1093–1103. [PubMed: 15466916]

Tang-Schomer MD, Johnson VE, Baas PW, Stewart W, Smith DH. 2012 Partial interruption of axonal transport due to microtubule breakage accounts for the formation of periodic varicosities after traumatic axonal injury. Exp. Neurol 233, 364–372. [PubMed: 22079153]

Walker DG, Lue LF. 2015 Immune phenotypes of microglia in human neurodegenerative disease: challenges to detecting microglial polarization in human brains. Alzheimer's Research & Therapy 7:56.

Wang J, Hamm RJ, Povlishock JT. 2011 Traumatic axonal injury in the optic nerve: evidence for axonal swelling, disconnection, dieback, and reorganization. J Neurotrauma 28:1185–1198. [PubMed: 21506725]

Wright RM, Post A, Hoshizaki B, Ramesh KT. 2013 A multiscale computational approach to estimating axonal damage under inertial loading of the head. J. Neurotrauma 30:102–118. [PubMed: 22992118]

Xu F, Huang J, He Z, Chen J, Tang X, Song Z, Guo Q, Huang C. 2016 Microglial polarization dynamics in dorsal spinal cord in the early stages following chronic sciatic nerve damage. Neuroscience Letters 617:6–13. [PubMed: 26820376]

Yi JH, Katagiri Y, Susarla B, Figge D, Symes AJ, Geller HM. 2012 Alterations in sulfated chondroitin glycosaminoglycans following controlled cortical impact injury in mice. J Comp Neurol 520:3295–3313. [PubMed: 22628090]

Zeng XX, Ng YK, Ling EA. 2000 Neuronal and microglial response in the retina of streptozotocin-induced diabetic rats. Vis Neurosci 17:463–471. [PubMed: 10910112]

Highlights

1. Focal cranial blast traumatic brain injury in mouse visual deficits
2. Focal cranial blast TBI causes optic nerve axon loss and retinal pathology
3. Focal cranial blast TBI activate retinal and optic nerve microglia to the M1 state
4. The cannabinoid type-2 inverse agonist SMM-189 ameliorates TBI visual system harm
5. SMM-189 benefit after TBI is associated with biasing of microglia to the M2 state

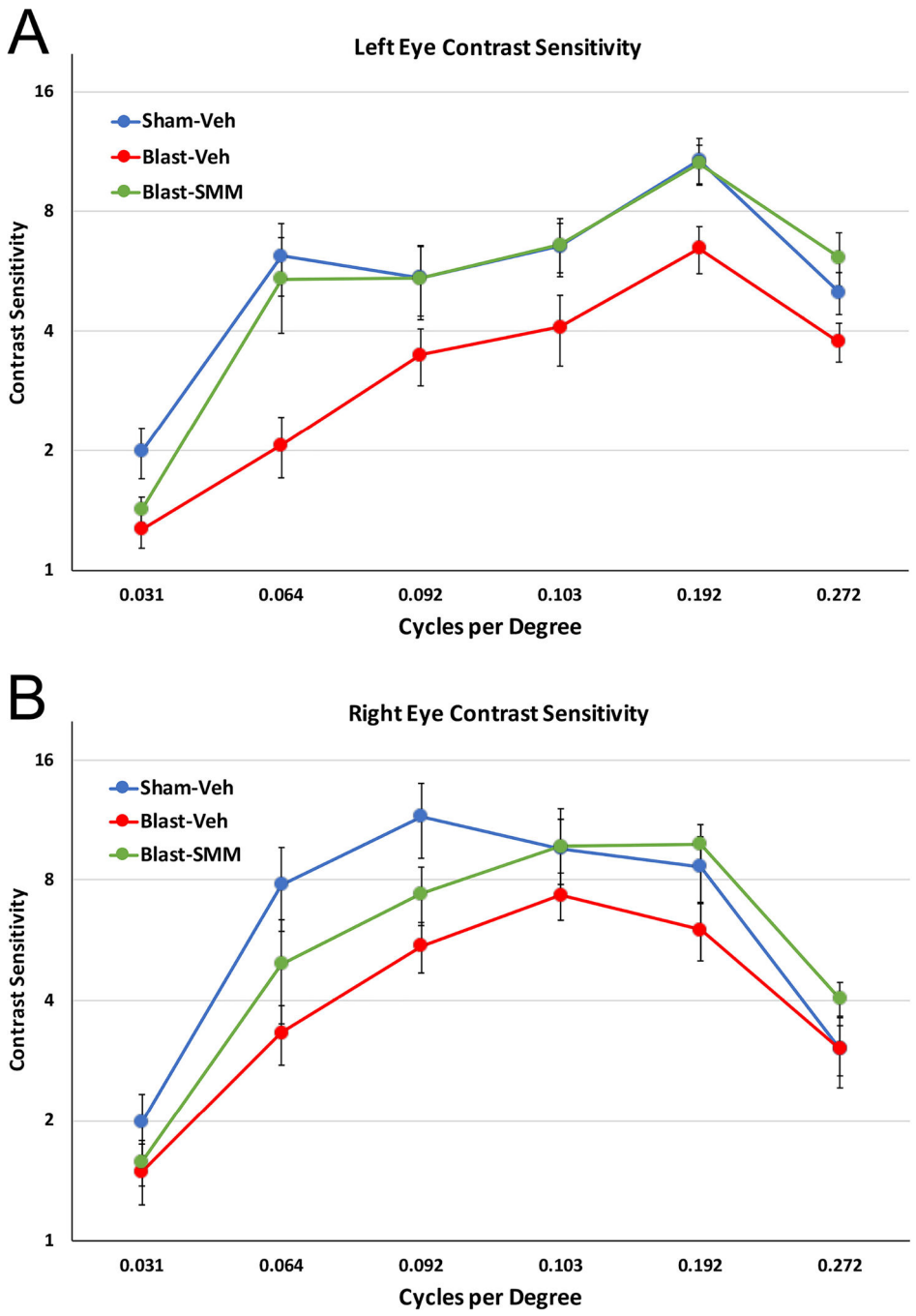

1. Contrast sensitivity functions of the left (A) and right eye (B) eye at 30 days after blast.
(A) The left eye of Blast-Veh animals (n=13) showed a prominent and significant deficit in contrast sensitivity across spatial frequencies compared to Sham-Veh animals (n=12) by two-way ANOVA ($p<0.0001$). This deficit was remedied with SMM-189 treatment, as indicated by the significant difference between the Blast-SMM group (n=13) and the Blast-Veh group ($p<0.0001$), but not between the Sham-Veh and the Blast-SMM group ($p=0.294$). (B) The right eye of Blast-Veh animals also exhibited a significant decrease in contrast sensitivity ($p=0.004$). This was significantly remedied by SMM-189 treatment, as contrast

sensitivity for the Blast-SMM mice differed from that of the Blast-Veh group (p=0.020), but not from the Sham-Veh group (p=0.470). Error bars are SEM.

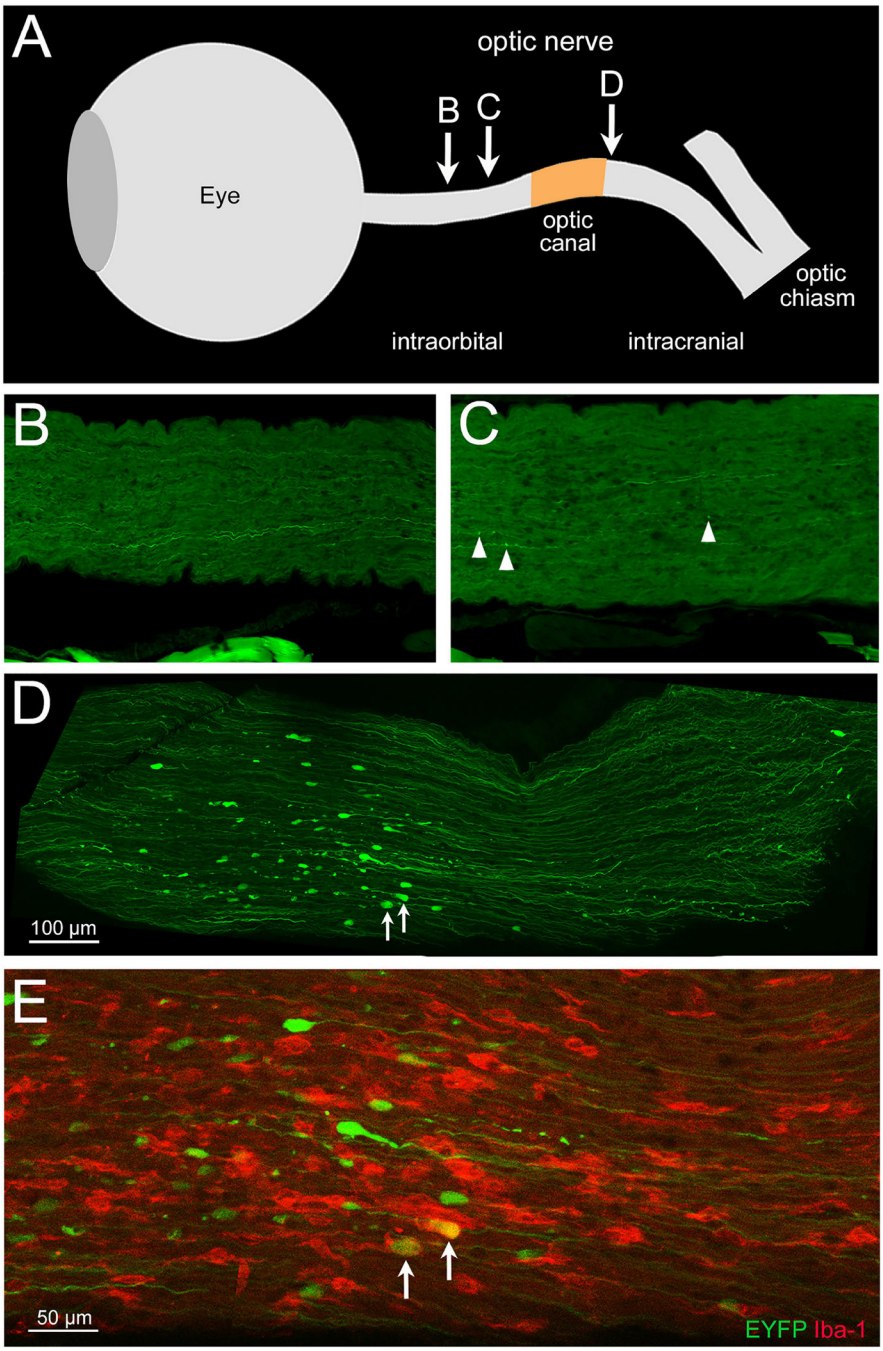

2. Localized injury in the left optic nerve

(A) Schematic view of the eye and optic nerve, constructed by overlaying a series of photographs taken during dissection and indicating the relative distances along the nerve between the eyeball, optic canal, and optic chiasm. The approximate locations of the images in panels B-E are based on overlays of low magnification images from consecutive cryostat sections, with the center of the eye used as a point of reference. (B-E) Confocal images of longitudinal sections from the left optic nerve of a vehicle-treated blast Thy1-EYFP reporter mouse 3 days after blast. For regions of optic nerve situated within the orbit (B and C), most

EYFP+ axons (green) appear intact, with little indication of axonal injury (B) or just a few scattered small axon bulbs (arrowheads in C). The pieces of tissue seen along the bottom of both images are strands of extraocular muscle fibers that acquired some autofluorescence during the extended storage of the tissue sections. The image in D shows numerous large axon bulbs occupying a 500 μm-long stretch of optic nerve, roughly corresponding to the cranial side of the optic canal. Fewer axon bulbs are present closer to the brain. E shows part of the same field of view as D at a higher magnification and immunolabeled for Iba-1, allowing visualization of microglia (red). The large axon bulbs are accompanied by intensely stained, microglia with short thick processes, two of which are seen engulfing axon bulbs (arrows). This area of injury may indicate a focal point of biomechanical forces exerted on the left optic nerve when the brain is displaced by the blast.

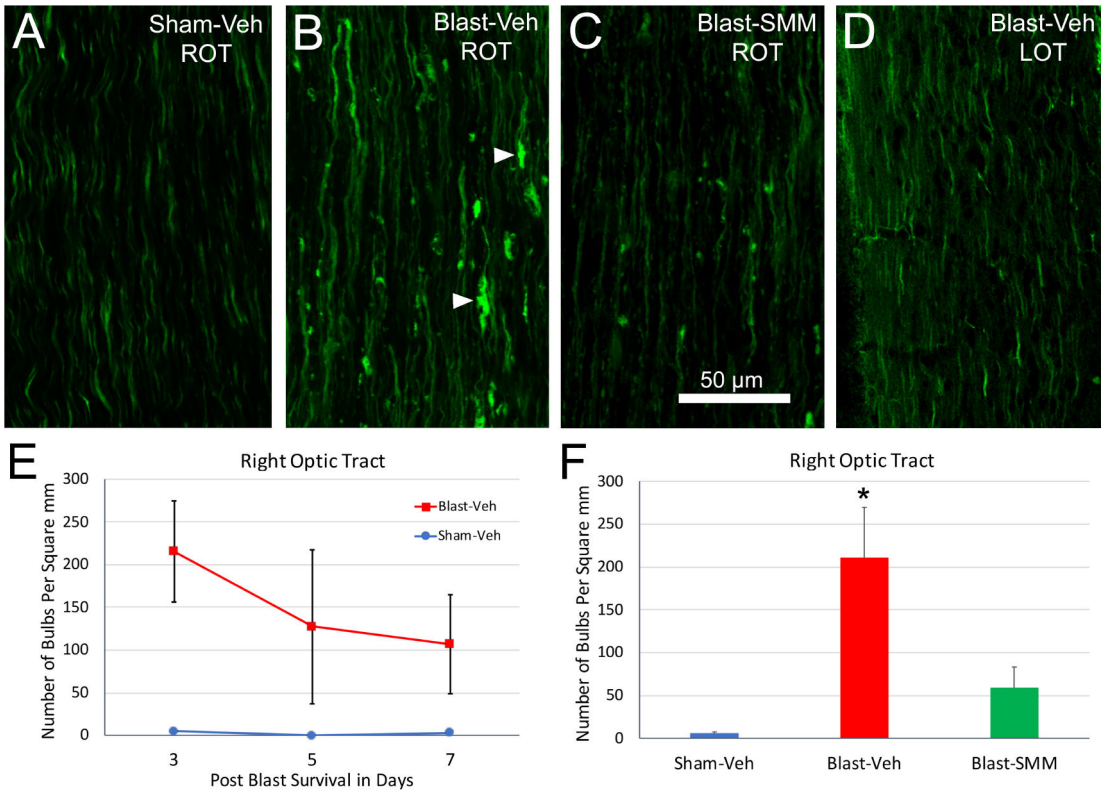

3. Axon bulbs in the optic tract following TBI.

(A-C). Sections from Thy1-EYFP reporter mice at 3 days post blast showing the right optic tract (ROT). (A) In Sham-Veh animals, EYFP+ axons are seen diving in and out of the plane of section and are relatively uniform in caliber. (B) In the Blast-Veh animals, by contrast, many EYFP+ axons appear swollen, and axon bulbs, indicative of disrupted axonal transport, are present (arrowheads). (C) Blast-SMM animals have fewer bulbs. (D) The left optic tract (LOT) in Blast-Veh mice has very few axon bulbs and resembles the left and right optic tracts of sham mice. The graph in E quantifies axon bulbs in the right optic tract at 3, 5 and 7 days after blast. Axon bulbs in the Blast-Veh animals are most abundant at 3 days (n=6), and then are progressively fewer at 5 (n=3) and 7 (n=2) days. The Sham-Veh animals had virtually no axon bulbs at 3 (n=5), 5 (n=1) and 7 (n=2) days. The number of bulbs in the Blast-Veh animals over the three days examined was significantly greater by two-way ANOVA than that in the Sham-Veh animals ($p=0.034$). The graph in F shows that drug treatment greatly decreases the number of axon bulbs in the right optic tract at 3 days after blast. Bulb abundance in Blast-SMM animals (n=3) is statistically equivalent to that in Sham-Veh animals, and is nearly significantly less than in Blast-Veh mice ($p=0.054$). Asterisk denotes that axon bulbs are more abundant in Blast-Veh than in Sham-Veh ($p=0.006$). Error bars are SEM. The scale bar in C applies to A-D.

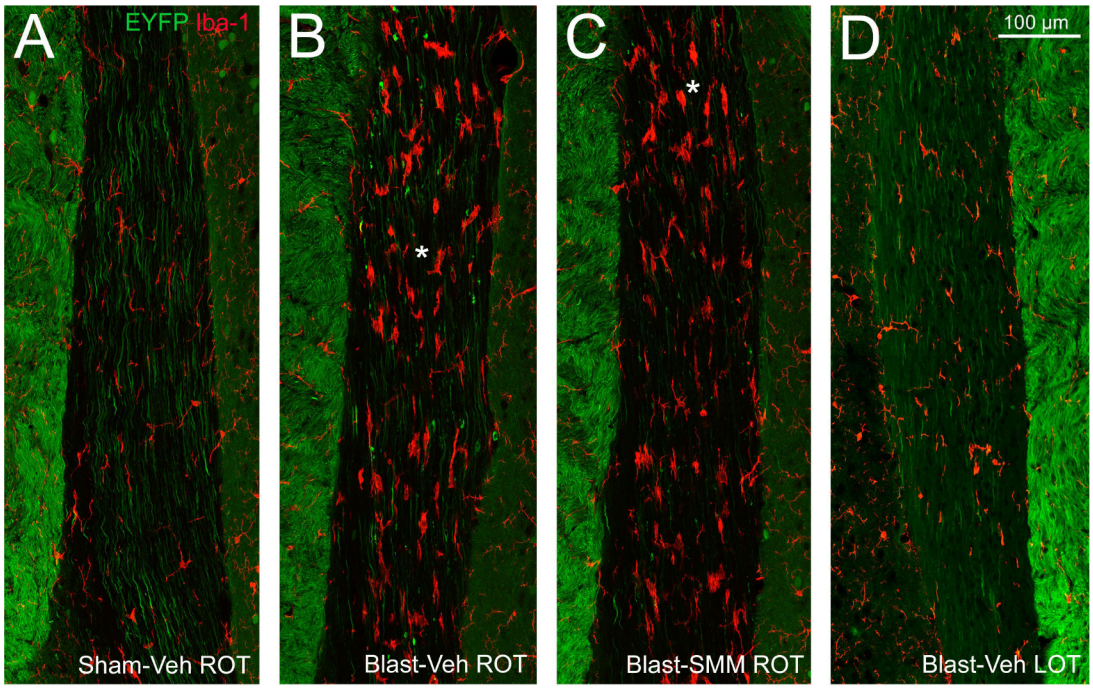

4. Axon bulbs and Iba-1+ microglia in the optic tract at 3 days post blast.

Sections from Thy1-EYFP reporter mouse 3 days after blast, immunolabeled for Iba-1, allowing visualization of microglia (red) and EYFP+ axons (green). (A) In Sham-Veh animals, EYFP+ axons in the right optic tract are of uniform caliber and most microglia have small cell bodies and thin processes. (B) In Blast-Veh mice, EYFP+ axon bulbs are common and most microglia have large cell bodies and short processes, all indications of traumatic axonal injury. (C) Blast-SMM animals have fewer axon bulbs and fewer reactive microglia. Asterisks in B and C indicate the regions of these same two sections analyzed for M1 versus M2 marker expression in Figure 5. (D). The left optic tract in Blast-Veh mice has very few axon bulbs and only few reactive microglia. Medial is to the left in A-C and to the right in D. The bright, densely packed EYFP+ axons seen medial to the optic tract are axons from the cerebral cortex descending in the cerebral peduncles. The scale bar in D applies to A-D.

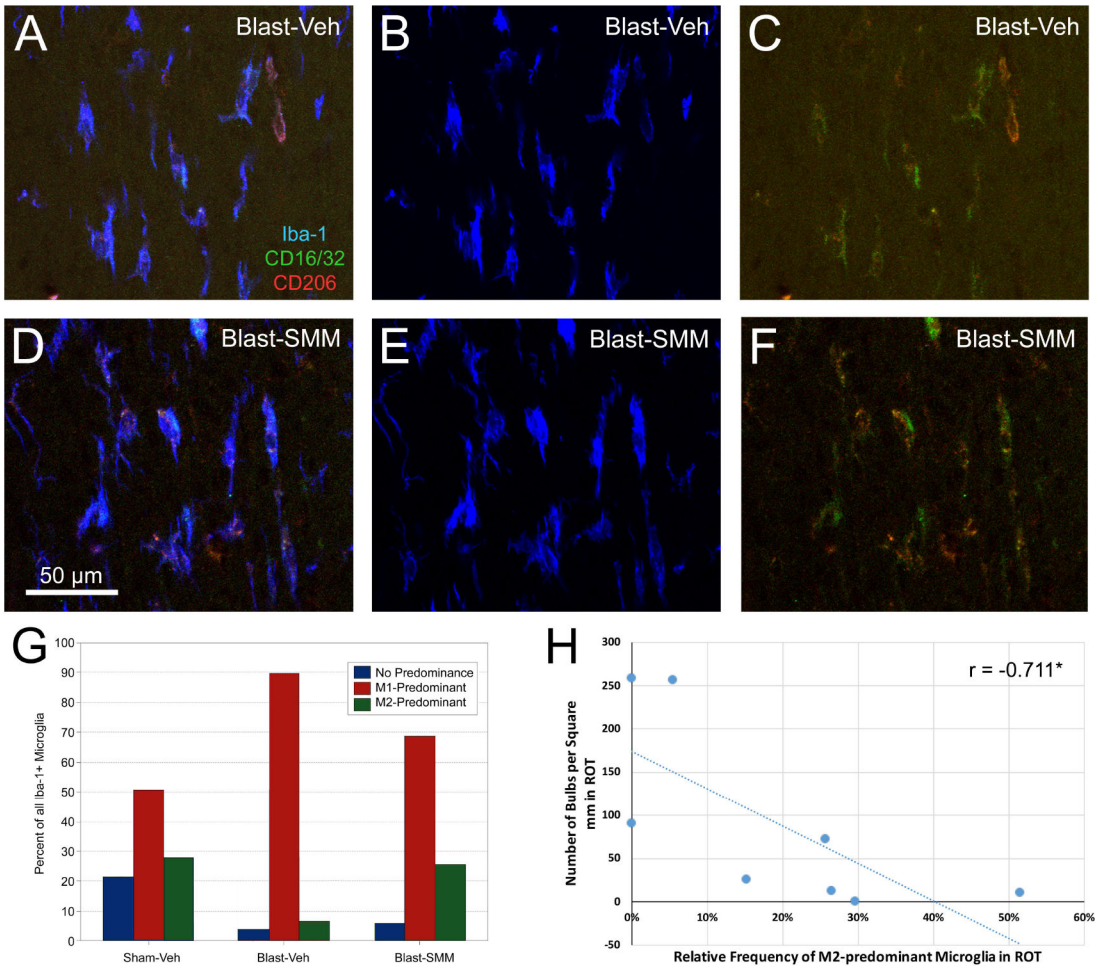

5. Microglial polarization in the right optic tract at 3 days after blast.

Sections through right optic tract of a Blast-Veh mouse (A-C) and a Blast-SMM mouse (D-F) from the same sections shown in Figure 4, simultaneously immunolabeled for Iba-1 (blue) to visualize microglia, for CD16/32 (green) to detect the M1 phenotype, and for CD206 (red) to detect the M2 phenotype. Panels A and D show the merge for all three markers, B and E show the Iba-1 channel alone, and C and F show the merge for the M1 and M2 markers. The green CD16/32 M1 labeling predominates more in the Blast-Veh blast image in C than in the corresponding Blast-SMM image in F, where the red CD206 M2 labeling is more readily seen. The scale bar in D applies to A-F. The graph in G quantifies the relative microglial polarization in the right optic tract based on immunostaining for CD16/32 (M1 marker) and CD206 (M2 marker). In sham mice, M1-predominant microglia made up about 50% of the microglia, with M2 and M0 about 25% each. By contrast, nearly 90% of microglia were M1-predominant in Blast-Veh mice. SMM-189 treatment reduced M1 predominance and increased M2 predominance compared to Blast-Veh mice, thus showing that SMM-189 biases microglia toward M2 polarization. The graph in H shows that M2-predominance and axon bulb abundance are inversely correlated and that the correlation is statistically significant (asterisk).

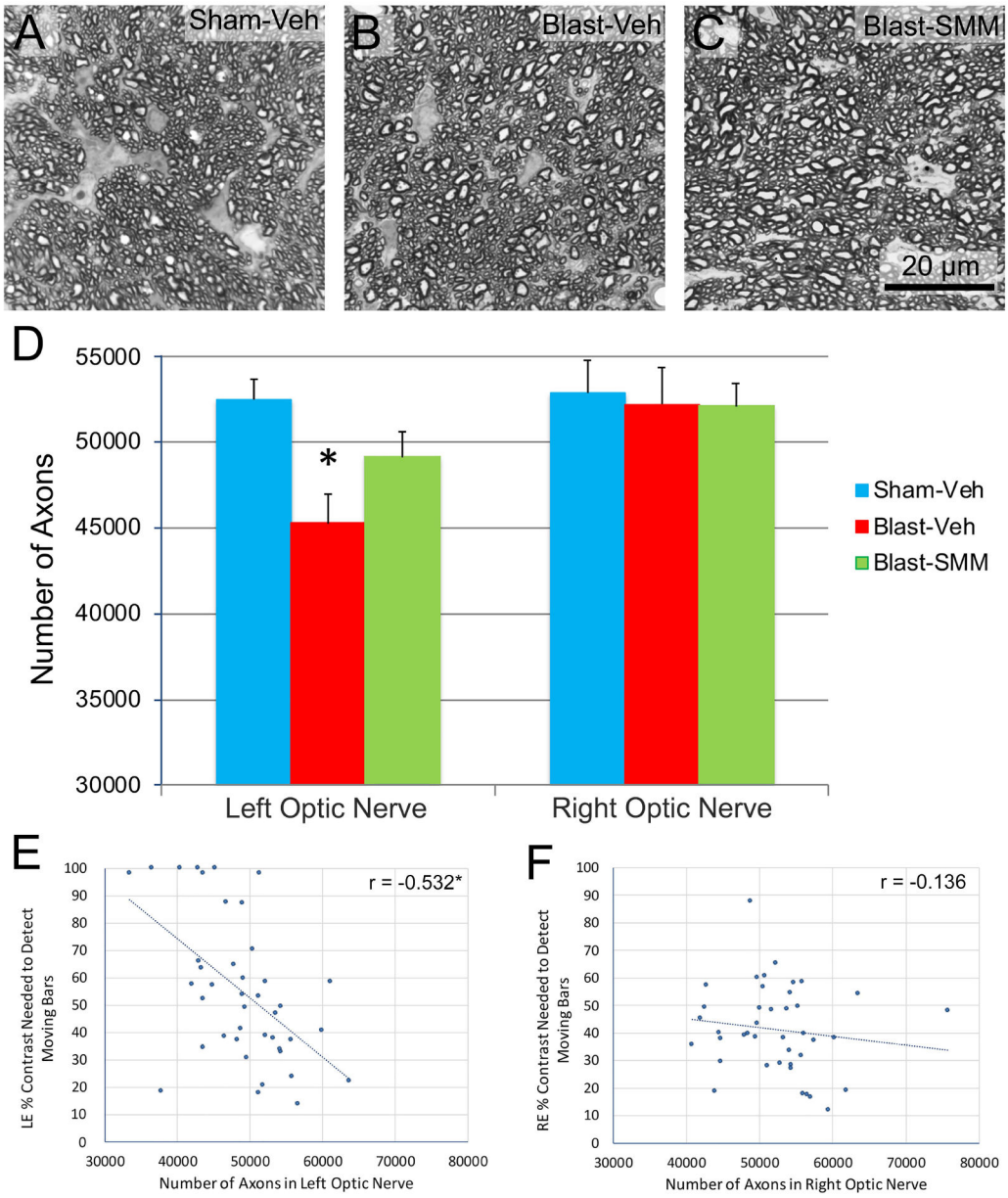

6. Optic nerve axon loss and rescue with SMM-189.

Panels A-C show high magnification views of the left optic nerves of Sham-Veh (A), Blast-Veh (B), and Blast-SMM (C) mice at >30 days post blast. No gross pathology is evident in the optic nerves after blast, with or without SMM-189 treatment. The scale bar in C applies to A-C. Axon counts (D) revealed ~10% significant loss of axons in the left optic nerve of Blast-Veh (n=14) (p=0. 0.002) compared to Sham-Veh left optic nerve (n=15), but not in the left optic nerve of Blast-SMM animals (n=13) (p= 0.139). No significant axon loss was seen in right optic nerve of Blast-Veh mice. The graphs in images E and F show the relationship between the number of optic nerve axons and the contrast sensitivity threshold for the left and right eye, respectively. The correlation for the left eye is significant (asterisk). Error bars in D are SEM.

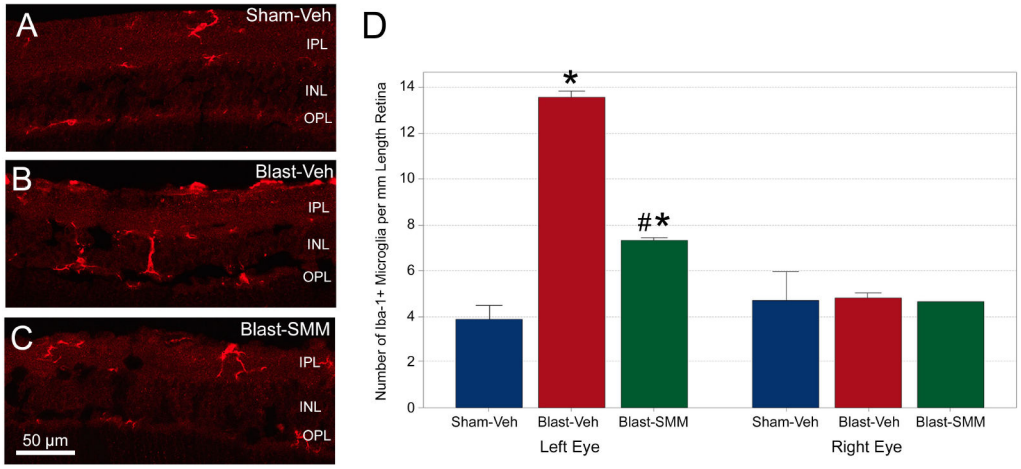

7. Microglia in the retina at 3 days after blast.

The images show Iba-1+ microglia in the left retinas of Sham-Veh (A), Blast-Veh (B), and Blast-SMM (C) animals. In Blast-Veh mice, microglia are more numerous than in Sham-Veh eyes, and more microglial processes cross the inner nuclear layer (INL) from the inner plexiform layer (IPL), with some extending into the outer plexiform layer (OPL). Left retinas from Blast-SMM animals have fewer microglia, but some microglial processes still extend into the OPL. The scale bar in C applies to images A-C. The graph in D quantifies the abundance of Iba-1+ microglia. The left eyes of Blast-Veh mice (n=3) show a large increase in microglial abundance (p=0.0004, asterisk) over Sham-Veh mice (n=2). SMM-189 treatment (n=3) remedied this, with microglial abundance significantly decreased compared to Blast-Veh mice (p=0.001, pound symbol), although microglia were still more numerous than after sham blast (p=0.008, asterisk). For the right eyes, microglial abundance is similar between experimental groups. (Note only one right eye was examined for Blast-SMM). Error bars are SEM.

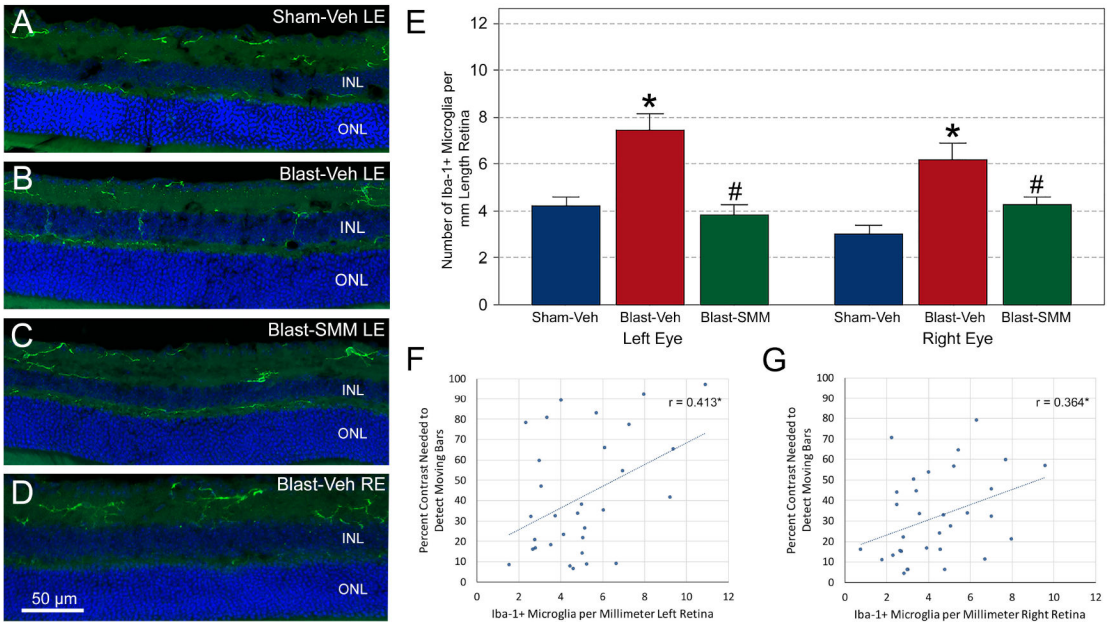

8. Microglia in the retina at 30 days after blast.

The images show Iba-1+ immunolabeled microglia in the left retinas of Sham-Veh (A), Sham-Veh (B), and Blast-SMM (C) mice, and the right retina of a Blast-Veh mouse (D). DAPI staining of cell nuclei is shown in blue. Microglia in both retinas of Blast-Veh mice are more numerous than in Sham-Veh eyes, with more microglial processes crossing the inner nuclear layer (INL) toward the outer nuclear layer (ONL). Left retinas from Blast-SMM animals had fewer microglia. The scale bar in D pertains to images A-C. The graph in E shows quantification of Iba-1+ microglia. Microglia in the left retina of Blast-Veh animals (n=9) are less abundant than at 3 days after blast, but are more abundant than in Sham-Veh controls (n=12; p=0.0001, asterisk). SMM-189 treatment (n=10) rescued this, with the left eye microglial counts for Blast-SMM mice being statistically indistinguishable from Sham-Veh mice, but significantly less than in Blast-Veh mice (p<0.0001, pound symbol). In contrast to the 3-day time point, the right eyes of Sham-Veh blast animals at 30 days showed a greater abundance of microglia than the Sham-Veh mice (p<0.0001, asterisk). SMM-189 treatment rescued this as well, with microglial abundance in Blast-SMM mice being significantly less than in Blast-Veh mice (p=0.011, pound symbol) and statistically indistinguishable from Sham-Veh mice. Error bars are SEM. The graphs in images F and G show the correlations between microglial abundance and contrast sensitivity thresholds for the left and right eyes, respectively. Both correlations are significant (asterisk).

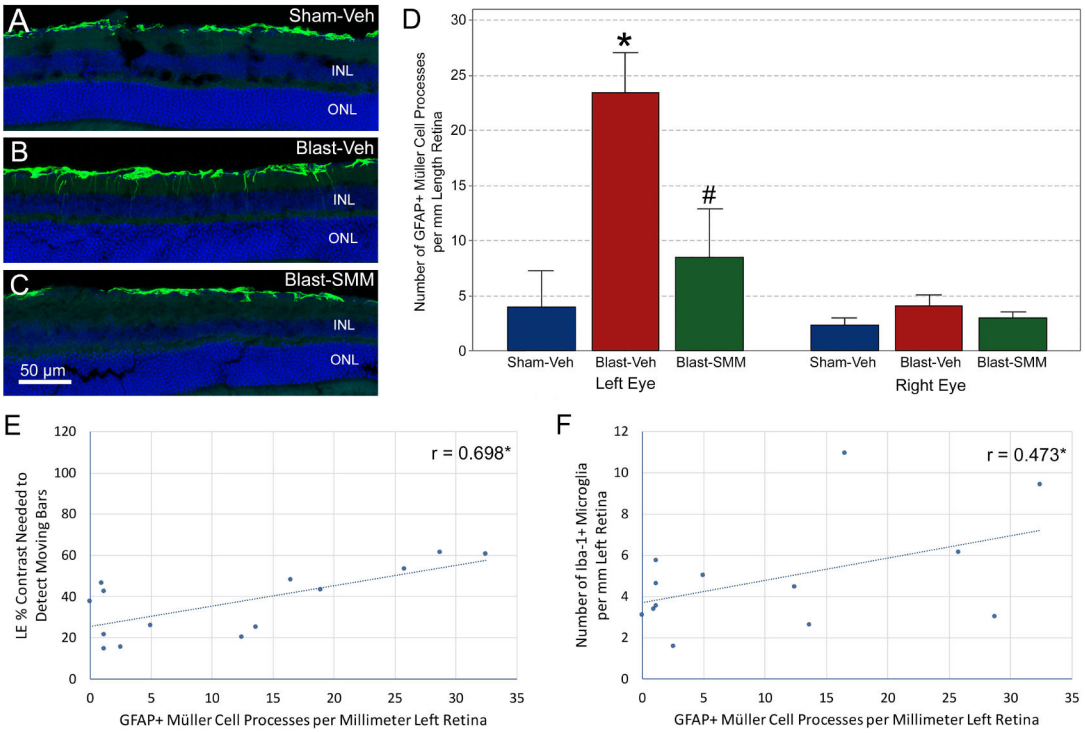

9. GFAP immunolabeling in the retina at 30 days after blast.

The images show GFAP immunostaining of retinal astrocytes and Müller glial cell processes in Sham-Veh (A), Blast-Veh (B), and Blast-SMM (C) mice. DAPI staining of cell nuclei is shown in blue. The Sham-Veh animals had a thin band of GFAP immunostaining in the nerve fiber layer (NFL), representing astrocytes and Müller cell end feet, interrupted by regions with little or no staining. In the Blast-Veh mice, GFAP immunolabeling of the NFL was more continuous, and numerous GFAP+ Müller cell processes crossed the inner plexiform layer (IPL) toward the inner nuclear layer (INL). The GFAP immunolabeling in Blast-SMM animals resembled that in Sham-Veh mice, with discontinuous NFL labeling and few Müller cell processes traversing the IPL. ONL = outer nuclear layer. The scale bar in C applies to A-C. The graph in D shows quantification of Müller cell processes crossing the IPL. The left retina of Blast-Veh mice (n=4) showed a clear increase (p=0.010, asterisk) in the number of crossing GFAP+ Müller cell processes compared to Sham-Veh mice (n=4). This was significantly remedied by SMM-189 treatment (n=6), as crossing GFAP+ processes were significantly fewer in Blast-SMM than in Blast-Veh eyes (p=0.024, pound symbol) and statistically indistinguishable from Sham-Veh mice. The number of crossing GFAP+ processes for the right eyes were similar for the three groups. Error bars are SEM. The graphs in images E and F show the correlation between left eye GFAP+ process counts and left eye contrast sensitivity thresholds and between left eye GFAP+ process counts and left eye microglial counts, respectively. Both correlations are significant (asterisk).

Table 1

Primary Antibodies used for Immunohistochemistry.

Antibody Target	Host	Antigen	Dilution	Source
SMI-32	Mouse Monoclonal	nonphosphorylated heavy neurofilament protein	1:2500	BioLegend
GFAP	Rabbit Polyclonal	50 kD GFAP purified from bovine spinal cord	1:100	Immunostar
Iba-1	Rabbit Polyclonal	synthetic peptide corresponding to Iba1 carboxy-terminal sequence	1:500	Wako Chemicals USA, Inc.
CD16/32	Rat Monocolonal	Epitope shared by CD16 and CD32	1:50	Abcam®
CD206	Goat Polyclonal	Leu19-Ala1388 sequence of recombinant mouse CD206	1:200	R&D Systems®, Inc.